

This article appeared in a journal published by Elsevier. The attached copy is furnished to the author for internal non-commercial research and education use, including for instruction at the authors institution and sharing with colleagues.

Other uses, including reproduction and distribution, or selling or licensing copies, or posting to personal, institutional or third party websites are prohibited.

In most cases authors are permitted to post their version of the article (e.g. in Word or Tex form) to their personal website or institutional repository. Authors requiring further information regarding Elsevier's archiving and manuscript policies are encouraged to visit:

<http://www.elsevier.com/copyright>



Contents lists available at ScienceDirect

Journal of the Mechanics and Physics of Solids

journal homepage: www.elsevier.com/locate/jmps

Regimes of frictional sliding of a spring–block system

Thibaut Putelat^{a,b,*}, Jonathan H.P. Dawes^c, John R. Willis^b^a Institute of Theoretical Geophysics, University of Cambridge, Centre for Mathematical Sciences, Wilberforce Road, Cambridge CB3 0WA, UK^b Department of Applied Mathematics and Theoretical Physics, University of Cambridge, Centre for Mathematical Sciences, Wilberforce Road, Cambridge CB3 0WA, UK^c Department of Mathematical Sciences, University of Bath, Bath BA2 7AY, UK

ARTICLE INFO

Article history:

Received 30 September 2008

Received in revised form

21 August 2009

Accepted 7 September 2009

Keywords:

Non-monotonic rate-and-state friction

Creep and inertial regimes

Stick-slip oscillations

ABSTRACT

In the context of rate-and-state friction, we revisit the crossover between the creep and inertial regimes in the dynamics of a spring–block system as observed and described in the dry friction experiment of Heslot et al. (1994) and Baumberger et al. (1994). We show that the transition between the quasi-static motion of a spring–block and its dynamic motion occurs at a lower sliding velocity than that which minimises the steady-state friction coefficient. We perform a weakly nonlinear stability analysis combined with numerical studies with the continuation package AUTO. In particular, attention is focused on the change of nature the Hopf bifurcation from supercritical to subcritical, as observed by Heslot et al. Comparing the results obtained for different friction laws, we conclude that the weakly nonlinear analysis provides a possible criterion for distinguishing which friction laws may be physically relevant.

© 2009 Elsevier Ltd. All rights reserved.

1. Introduction

A few decades ago, friction experiments performed on rocks, by Dieterich (1979) in particular, led Ruina (1980), Rice and Ruina (1983) to formalise the concept of rate-and-state friction. On a frictional interface, this kind of friction law relates the shear stress τ to the normal stress σ and the slip rate v while memory effects are taken into account through state variables ϕ which evolve according to empirical evolution equations. These internal variables model the complex interactions between the asperities which constitute the frictional interface. For the sake of simplicity, only one state variable is considered here. Following Rice et al. (2001), a rate-and-state friction law can formally be written as

$$\begin{cases} \tau = F(v, \phi; \sigma), \\ \dot{\phi} = -G(v, \phi). \end{cases} \quad (1)$$

In this study, the normal stress is considered as a constant parameter, its influence as a variable, especially on the interfacial state, being disregarded.

Information on the friction law can be gained from a spring–block system for which a block of mass M is pulled over a flat surface with a spring of stiffness k driven at a specified velocity $V(t)$. Denoting by $x(t)$ the position of the block and $X(t) - x(t)$ the extension of the spring, so that $\dot{X}(t) = V(t)$, the motion of the block is governed by

$$M\ddot{x} = k(X - x) - \tau. \quad (2)$$

* Corresponding author at: ITG, University of Cambridge, Centre for Mathematical Sciences, Wilberforce Road, Cambridge CB3 0WA, UK.
E-mail address: T.Putelat@damtp.cam.ac.uk (T. Putelat).

When V is constant and the sliding is steady, the inertia of the block plays no role and (1) must lead to a steady-state expression $\tau = F_{ss}(V; \sigma) = F(V, \phi_{ss}(V); \sigma)$ obtained in combination with $G(V, \phi_{ss}) = 0$. Interestingly, for a rather wide range of slip rates roughly from $\approx 10^{-2} \mu\text{m s}^{-1}$ to $\approx 1 \text{ mm s}^{-1}$, it has been recognised that friction of rocks, metals and other solids shows a velocity weakening with a logarithmic dependence (for rocks see Dieterich, 1979; Ruina, 1983; Marone, 1998; Scholz, 2002; Heslot et al., 1994 for Bristol paper and Rabinowicz, 1995 for metals). In this velocity-weakening regime, the steady state becomes unstable, giving way to a dynamic oscillation, if the spring constant k is less than a critical value k_c . While some information about the partial derivatives of F and G can be experimentally inferred from the response to a velocity jump, it is mostly the steady-state friction law which can be measured via the extension of the spring.

In addition to this generic feature of dry friction, it has also been observed that the steady-state friction is a non-monotonic function of the slip rate, presenting a velocity strengthening at very low and high slip rates (Shimamoto, 1986; Heslot et al., 1994; Rabinowicz, 1995 for instance). By reducing slip rates, Shimamoto (1986) found for halite a transition from the logarithmic velocity weakening frictional regime towards a strengthening one where ductile shear is activated along the interface. On the other hand, for very high slip rates, when heat produces partial melting, Tsutsumi and Shimamoto (1997) showed another velocity weakening effect of the type that Bowden and Freitag (1958) observed with metal.

Because in situations such as earthquake mechanics (Scholz, 2002) the slip-rate span involved is wide, it is appealing to describe different regimes of friction at once using a single friction law. In addition, the constraints obtained by this phenomenological approach give interesting insights for the microscale description and discrimination of the physical mechanisms involved in the friction phenomenon. The rate-and-state formalism (1) is a good candidate to achieve these purposes as we show in this paper by revisiting the experimental results for Bristol paper friction obtained by Heslot et al. (1994) and Baumberger et al. (1994, 1995). We refer to these papers collectively as Heslot et al. in the remainder of this paper. Our aim is to reconcile the phenomenological steady-state kinetic friction law inferred from Heslot et al.'s experiments with the dynamic behaviour of the spring–block system modelling the friction force apparatus used for the measurements. As explained below, this requires us to probe the interplay between the crossover from the quasi-static sliding regime to the inertial one and the change of monotonicity of the steady-state friction coefficient in relation with the stick-slip instability onset. The effects of inertia are included in our analysis.

We now briefly summarise the experimental results of Heslot et al. and their theoretical explanation. We then discuss where further consideration may be needed and outline our more detailed analysis presented in this article.

Investigating the sliding dynamics of a spring–block system, Heslot et al. (1994) have experimentally established that the variation with the driving velocity V of the steady-state friction coefficient $\mu_{ss}(V) = F_{ss}/\sigma$ evolves from a velocity-weakening part at low slip rates, where it decreases, to a strengthening part at high slip rates (cf. Fig. 1(a)). The weakening part, corresponding to a *creep regime* as they denote it, varies in first approximation as the logarithm of V , whereas the so-called *inertial regime* corresponding to the strengthening part is a linear function of V . This experimental result shows that the steady-state friction coefficient reaches a local minimum for a slip rate V_m on the order of mm s^{-1} . In addition, the nature of the stick-slip instability apparently changes at a slip rate V^* of about $2 \times 10^{-5} \text{ m s}^{-1}$ (cf. Fig. 1(b)). At low slip rates $V < V^*$, the onset of stick-slip oscillations corresponds to a supercritical Hopf bifurcation, whereas at higher slip rates, the

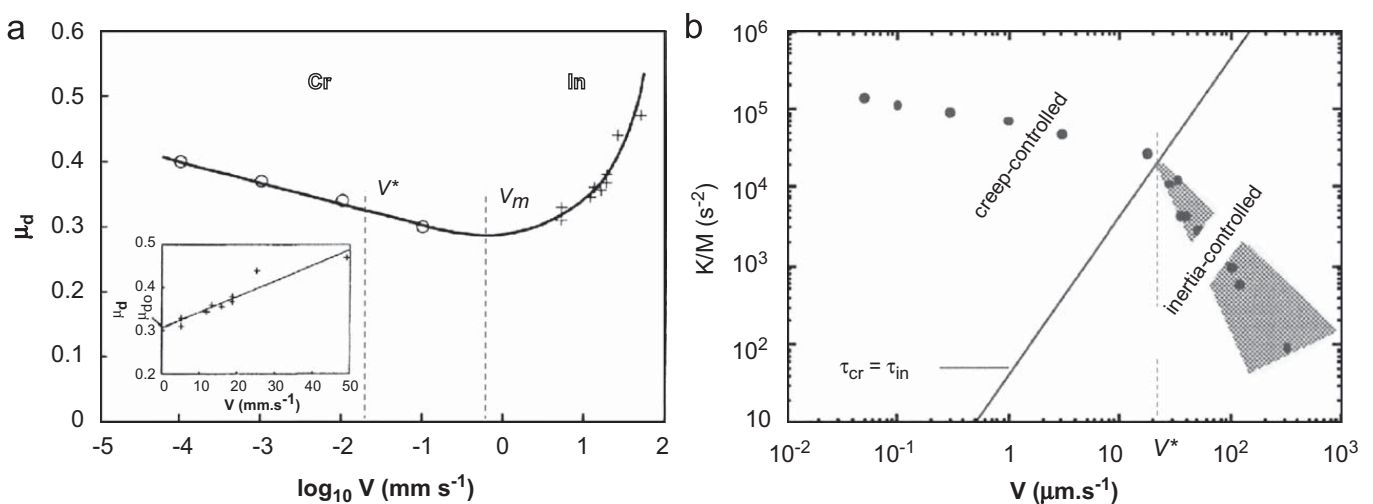


Fig. 1. Experimental results from Heslot et al.: (a) Steady-state kinetic friction coefficient $\mu_d(V)$ showing a transition from a logarithmic velocity-weakening regime to a linear velocity-strengthening one; we denote by V_m the slip rate at which $\mu_d(V)$ is minimum. (Reproduced from Heslot et al., 1994 Fig. 4.) (b) Stability regime diagram ($V, k/M$) illustrating the change in the nature of the stick-slip bifurcation at V^* from a supercritical one at low slip rates to a subcritical bifurcation at higher slip rates. (Reproduced from Baumberger, 1996, Fig. 15.) Heslot et al. (1994) suggest that this change of behaviour is related to the change of the monotonicity of the steady-state dynamical friction coefficient. They argue furthermore that it corresponds to the crossover from a so-called creep regime (Cr) to an inertial one (In) where the inertia is no longer negligible in the momentum conservation equation of a spring–block system.

bifurcation is interpreted as a subcritical Hopf bifurcation associated with the appearance of a hysteresis phenomenon and large amplitude stick-slip oscillations. Thus Baumberger et al. (1994) indicate that steady-state sliding in the inertial regime, although linearly stable, is unstable to finite amplitude perturbations. The same authors also claim that “the inertial regime and the associated velocity strengthening behaviour is system-dependent” and argue that their experiment shows that the system controls the onset of the inertial regime because they consider that $V_m = V^*$. This defines a unique slip rate splitting the creep and inertial regimes and which varies with the ratio k/M . Indeed, their analysis is based on the comparison between two time scales involved in the problem (Rice and Tse, 1986): the characteristic time of the free oscillations of the system $\tau_{in} = \sqrt{M/k}$ and a characteristic time $\tau_{cr} = L/V$ over which the state variable reaches its steady-state value. The characteristic length L is usually interpreted as the memory length necessary for the rejuvenation of the population of interfacial contacts, that is, the slip distance over which $\phi \rightarrow \phi_{ss}$ (e.g. Marone, 1998). The transition between the two regimes arises when $\tau_{in} \approx \tau_{cr}$ which then defines the transitional slip rate V^* via $V^*(k/M) = L\sqrt{k/M}$.

In disagreement with the interpretation of Heslot et al. we believe that V^* does not correspond to the transition at V_m between the velocity-weakening/velocity-strengthening regimes of friction. First note that V^* and V_m are separated by around two orders of magnitude in the present situation. Crucially, moreover, the whole shape of the steady-state friction coefficient, and consequently V_m , cannot depend on the stiffness k because these measurements are obtained in steady-state sliding. The existence of the transition from the velocity weakening regime to the velocity strengthening regime suggests that the slip-rate V_m is an intrinsic feature of the friction phenomenon corresponding to a change in the nature of the interactions between the microscopic asperities forming the frictional interface. It is indeed intuitively reasonable to imagine that different mechanisms of asperity deformation are activated in relation to the slip rate at which an interface slides, resulting in a friction force which varies in a non-monotonic manner with the velocity. For example, considering different models of asperity interactions, Estrin and Bréchet (1996) proposed physical models of rate-and-state friction exhibiting such transitions between velocity weakening and strengthening behaviours. Note moreover that the experimental results of Kilgore et al. (1993) suggest that the location of V_m can be controlled by varying the imposed normal stress; the location of a local minimum of the friction coefficient moves towards higher slip rates as the normal stress increases. From this perspective, a mass dependence of V_m through the normal stress Mg is conceivable, inertia playing no role in steady sliding.

On the other hand, the stick-slip oscillations of the block, arising from an unstable steady-state sliding, do not seem consistent with this change of monotonicity of the steady-state friction coefficient $\mu_{ss}(V)$. Indeed, the steady slip of the block becomes linearly unstable for stiffnesses smaller than a critical value k_c which is proportional to the slope $\mu'_{ss} \equiv d\mu_{ss}/dV$ of the steady-state friction coefficient (Ruina, 1980; Rice and Ruina, 1983). In the rate-and-state context (1) with $F(v, \phi; Mg) = Mg\mu(v, \phi)$, the critical stiffness of the spring-block system (2) is given by

$$k_c = -MgG_\phi\mu'_{ss} (1 + MG_\phi/(Mg\mu_v)), \quad (3)$$

where μ_v and G_ϕ denote the partial derivatives of μ and G with respect to v and ϕ and evaluated for a steady-state $(V, \phi_{ss}(V))$. Therefore we must have $k_c(V_m) = 0$ and when $V > V_m$, where friction strengthens with slip rate, steady sliding must be linearly stable for all k . Yet, Fig. 1(b) shows that $k_c(V^*)/M \approx 2 \times 10^4 \text{ s}^{-2}$ which contradicts the hypothesis $V^* = V_m$ considered by Heslot et al. Comparison of Figs. 1(a) and (b) would be problematic if, for instance, Heslot et al. performed the experiments at high velocities using a different mass, since this could well alter the friction law through change in the normal stress Mg . Unfortunately, only partial information is available in Heslot et al. (1994), Baumberger et al. (1994), and Baumberger (1996) about the experimental conditions which led to the two results in Fig. 1. For instance, it would have been very interesting to show the effects of the mass M and the stiffness k on the measurement of the dynamical steady-state friction coefficient to demonstrate experimentally how V_m is shifted. Heslot et al., however, comment that the experiment is difficult to perform when inertia plays a role. A lot of noise is observed and the boundary of the onset of stick-slip oscillations is fuzzy. This could also cause another source of mismatch between V^* and V_m if the noise amplitude is at least of order of the stick-slip oscillations in the neighbourhood of the instability onset.

Nevertheless, in our opinion, the simplest way of reconciling the discrepancy between the two results in Fig. 1, assuming that $V^* \neq V_m$, is to investigate a change in nature of the Hopf bifurcation that generates stick-slip oscillations originating from nonlinear effects due to the friction law, possibly combined with effects of inertia, but still inside the domain of velocity-weakening friction. Considering a friction force which is non-monotonic intrinsically, we seek a better understanding of the effect of inertia on the development of frictional sliding instabilities. To do so, we present a general weakly nonlinear analysis of the stability of a spring-block system. In contrast to a linear stability analysis which reveals only the existence and location of a bifurcation in parameter space (and, for a Hopf bifurcation, the frequency of small oscillations), a weakly nonlinear analysis allows the nature (super- or sub-critical) of the bifurcation to be identified from the derivation of a so-called amplitude equation which governs the variation of the amplitude of instabilities away from the bifurcation point. As a result we are able to explain why the nature of the Hopf bifurcation changes and to provide quantitative predictions for the amplitude of the oscillations when parameters are varied (Drazin, 1992). In the present context, we have in mind that the coefficient \mathcal{A} of the nonlinear term in the amplitude equation of the Hopf bifurcation $d|A|^2/dT = \Gamma|A|^2 + \mathcal{A}|A|^4$ could change its sign depending on the value of the slip rate (cf. Fig. 2). As a consequence, in agreement with the experimental observations, the nature of the Hopf bifurcation could change from a supercritical one ($\mathcal{A} < 0$) to a subcritical one ($\mathcal{A} > 0$) along the critical curve $k_c(V)$ which delimits the region of linear stability in the phase

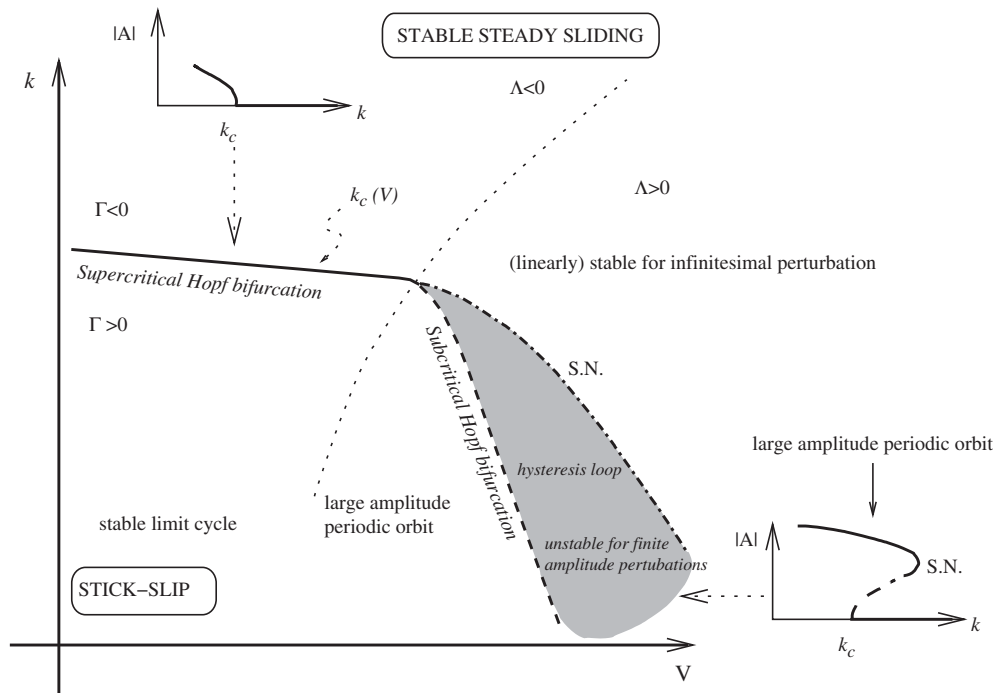


Fig. 2. A phase diagram giving a possible explanation of the change in nature of the Hopf bifurcation from supercritical (—) to subcritical (---) as observed by Heslot et al. (1994): when the Hopf bifurcation is subcritical, an unstable periodic orbit grows and becomes stable after a saddle-node bifurcation (S.N., - - - -) giving birth to large amplitude oscillations. Between the Hopf and the saddle-node bifurcation, a domain of bistability exists where the steady-state sliding is unstable to finite size perturbations, leading possibly to hysteretic cycles. This change of nature of the Hopf bifurcation is related to a change of sign of the Landau coefficient (dotted line) in the amplitude equation obtained in the vicinity of the critical stiffness $k_c(V)$ of the stick-slip oscillation onset (Eq. (3)).

diagram (V, k) . In addition, it is possible that inertia could be responsible for reducing the amplitude of the oscillations to the order of magnitude of the experiment noise so that the dynamics would not be distinguishable.

The structure of the remainder of the paper is as follows. After the formulation of the problem and general comments on the spring–block dynamics, we develop the weakly nonlinear stability analysis taking into account the block inertia. Next, successively considering purely monotonic friction laws of the Dieterich–Ruina type, and then three non-monotonic ones, we examine the variations with velocity of the coefficients of the amplitude equation and the associated growth rate and amplitude of stick-slip oscillations in order to analyse how the friction law and inertia determine the nature of the Hopf bifurcation. A fully nonlinear bifurcation analysis performed with the continuation package *Auto* completes and confirms these analytical results. Finally, a discussion and comparison with experimental observations is presented.

The central conclusion of the paper is that the merits of one friction law over another should be examined not just by analysing the steady-state friction coefficient that each friction law implies, but also by examining the dynamical behaviour that each gives rise to. The weakly nonlinear analysis that we carry out in this paper is an important step in the investigation of the dynamical behaviour given by different friction laws enabling us to compare the instabilities associated with different rate-and-state friction laws with the response observed in experiment.

2. Theoretical framework

2.1. Equations of motion and stick-slip cycle

A block of mass M is pulled over a flat and horizontal frictional surface at a constant speed V through a spring of stiffness k . In a fixed frame of reference, $x(t)$ gives the position of the block sliding at the velocity $\dot{x}(t)\mathbf{i}$. Neglecting vertical motion and the effects of fluctuations of the normal stress, the dynamics of such a spring–block system with rate-and-state friction is determined by

$$\begin{cases} M\ddot{x} = k(Vt - x) - F(\dot{x}, \phi; \sigma), \\ \dot{\phi} = -G(\dot{x}, \phi), \end{cases} \quad (4)$$

where the normal stress $\sigma = Mg$ is held constant. It is interesting to reformulate this system in terms of a set of first order differential equations to go further in the physical understanding and the numerical analysis of this system than the one brought by just considering the two characteristic time scales τ_{cr} and $\tau_{in} \equiv \sqrt{M/k}$.

To this end, let us denote the spring force by $y = k(Vt - x)$ and the sliding velocity $v = \dot{x}$. Furthermore, measuring length, time and force in units of L , L/V_* and Mg , respectively, the dimensionless form of Eqs. (4) reads with a slight abuse of

notation

$$\begin{cases} \dot{y} = \kappa(V - v), \\ \dot{\phi} = -G(v, \phi), \\ m \dot{v} = y - \mu(v, \phi), \end{cases} \quad (5)$$

where the dimensionless mass m and stiffness κ are defined by

$$m = V_*^2/(gL) \quad \text{and} \quad \kappa = kL/(Mg). \quad (6)$$

As introduced in the next section, the velocity V_* considered here is a reference slip rate associated with a reference value of the steady-state coefficient of friction. Also, the length L is characteristic of the length of slip after which a steady state is attained following a step change in slip velocities.

The instantaneous friction coefficient $\mu(v, \phi)$ corresponds to a dimensionless friction force, Eqs. (5), directly leading to the system which describes the motion in the quasi-static approximation of a single frictional interface between two elastic layers, on setting $m = 0$ (Rice and Ruina, 1983; Gu et al., 1984). Taking into account the block inertia couples the spring and friction forces in a subtle way. The dynamics of the block is indeed determined by the interplay of the three variables y , ϕ and v over different phases we describe relative to the characteristic time $L/V_* = O(1)$ scaled by reference to the evolution of the state variable ϕ . In the context of the experiment of Heslot et al., there is a hierarchical relation between y , ϕ and v . They correspond, respectively, to the slow, intermediate and fast variables of the system.

This hierarchy is a consequence of the orders of magnitude of the parameters m and κ . Unless the acceleration of gravity g is changed, the dimensionless mass m is fixed once a given material is chosen, setting the frictional properties V_* and L . For the Bristol paper board used by Heslot et al. (1994), $L \approx V_* \approx 10^{-6}$ which implies a very small dimensionless mass: $m \approx 10^{-7}$. In contrast, the mass M of the block and the spring stiffness k can be easily modified. In the experiment of Heslot et al., the ratio k/M broadly varies between 10 and 10^6 s^{-2} . Then, as $L/g \approx 10^{-7} \text{ s}$, the dimensionless stiffness varies over several orders of magnitude: $10^{-6} \leq \kappa \leq 10^{-1}$. We then expect fully developed stick-slip dynamics to be governed by the limits $m \ll 1$ and $\kappa \ll 1$.

Putelat et al. (2008) addressed this point of view while building a composite approximation of the stick-slip cycle inspired by the picture of stick-slip oscillations drawn by Rice and Tse (1986). They indeed decompose the stick-slip cycle into two main phases of different duration: a long quasi-static “stick” stage where the friction force balances the spring force increase is followed by a short dynamic slip phase controlled by inertia and accompanied by an elastic stress drop governing an overshoot at constant state which ends the cycle and determines the block “arrest”. Interestingly, during the dynamic phase, a peak in the block slip rate is achieved along $\mu_{ss}(v)$ as the state evolves on $\phi_{ss}(v)$ due to the fast state relaxation promoted by the rapid block sliding. Fig. 3 illustrates such a cycle.

Rice and Tse (1986) argued that these two phases can be distinguished from the comparison of the inertial and state relaxation time scales, the latter one based on the actual slip velocity v , i.e. $\tau_{cr}(v) = L/v$; hence the ratio $\tau_{in}/\tau_{cr}(v)$ evolves along one cycle between the extremes $\ll 1$ (quasi-static “stick” stage) and $\gg 1$ (inertia-controlled dynamic slip). For numerical time integration purposes, this separation of time scales allows them to reduce the full system of governing equations, derived from (4), to quasi-static and dynamic approximations, valid under further hypotheses of considering that the time of “stick” is much larger than the natural vibration period $2\pi\sqrt{M/k}$ and that the slip is much greater than the relaxational slip distance L . Interestingly, provided that the block acceleration is much less than v^2/L , it is shown that the

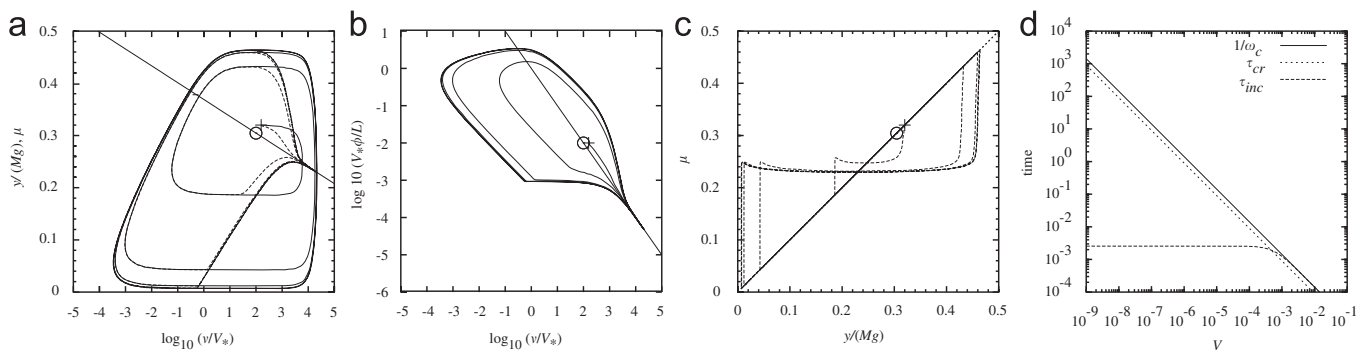


Fig. 3. (a–c) A typical stick-slip cycle computed from the time integration of the spring–block Eqs. (5) under the Dieterich law (26)–(28) for $V/V_* = 10^2$ and $kL/(Mg) = 10^{-3}$: the dimensionless friction force μ (---) is first balanced by the build-up of the dimensionless spring force $y/(Mg)$ (—) during a long quasi-static “stick” phase, then a short dynamic phase occurs which is controlled by inertia and is characterised by a friction drop and the block’s acceleration; finally this is followed by an overshoot which controls the block arrest. Symbols: initial condition (+), equilibrium (θ), steady states locus (thin solid line). (d) Variation of the characteristic time-scales with the driving velocity V for the Dieterich–Ruina laws (26), (28), (29): state relaxation time $\tau_{cr} = L/V$, critical stick-slip period $2\pi/\omega_c = 2\pi\sqrt{a/(b-a)}L/V$, critical free oscillation time $\tau_{inc} = \sqrt{M/k_c} = [g(b-a)(1+V^2/agL)/L]^{-1/2}$. Steady-state sliding is unstable when $\sqrt{M/k} = \tau_{in} \geq \tau_{inc}$. At the onset, the characteristic time-scale of stick-slip oscillations $1/\omega_c$ is of order of the state relaxation time-scale $\tau_{cr}(V)$ which are much larger than τ_{inc} for slow driving.

dynamic approximation leads to harmonic oscillations because the friction force varies slowly as $F_{ss}(v)$, and can be considered to be constant over a short range of v .

We deduce from these results that it is inappropriate to evaluate the effect of inertia on the block motion by choosing the driving velocity V as a characteristic velocity scale to define the state relaxation time and compare it to the inertial time. Even at low driving velocity, i.e. $V \ll L/\sqrt{M/k}$, inertia cannot be neglected and controls slip events by preventing their finite time blow up. However, as this point of view is only valid far from the instability onset, it is still relevant to question the role of inertia in the initial development of stick-slip dynamics. To this end, we must analyse the stick-slip amplitude.

2.2. The amplitude equation

Inspired by the method and notations of [Baumberger et al. \(1995\)](#), we perform a weakly nonlinear stability analysis in order to find the amplitude equation which determines the stick-slip amplitude in the vicinity of the instability threshold.

The steady-state solution (x_0, ϕ_0) of (4) is given by

$$k(Vt - x_0) = F(V, \phi_0; \sigma), \quad G(V, \phi_0) = 0,$$

and becomes unstable at a Hopf bifurcation point (Rice and Ruina, 1983; Gu et al., 1984; Heslot et al., 1994; Lim and Chen, 1998) when the stiffness is smaller than a critical stiffness k_c given by (3) and written here as

$$k_c = (F_\phi G_V - F_V G_\phi)(1 + MG_\phi/F_V), \quad (7)$$

where subscripts on the right-hand side denote partial derivatives. Note that $F_\phi G_V - F_V G_\phi = -G_\phi F'_{ss}(V)$. The frequency at the onset of the instability is given by

$$\omega_c^2 = \frac{k_c G_\phi}{F_V + MG_\phi} = -\frac{G_\phi^2 F'_{ss}(V; \sigma)}{F_V}. \quad (8)$$

It is remarkable that this frequency is determined only by the frictional properties of the interface.

In the neighbourhood of the bifurcation point, we seek a weakly nonlinear solution from a multi-scale development of x and ϕ assuming a long time scale $T = \varepsilon^2 t$ and expanding the stiffness $k = k_c + \varepsilon^2 k_2$ where ε is a small parameter. We expand x and ϕ similarly:

$$x = x_0(t) + \sum_{n \geq 1} \varepsilon^n X_n(t, T), \quad (9)$$

$$\phi = \phi_0 + \sum_{n \geq 1} \varepsilon^n \phi_n(t, T), \quad (10)$$

where $x_0(t) \equiv Vt - F(V, \phi_0; \sigma)/k$ and ϕ_0 comprise the steady-state solution of (4). These asymptotic expansions together with the Taylor expansions of F and G around the steady state lead to linear systems of equations at each order in ε . At $\mathcal{O}(\varepsilon^3)$, the Fredholm condition and the cancelling of secular terms yield a Landau equation for the amplitude of the leading order solution.

At first order, (4) reads

$$\begin{pmatrix} M \frac{\partial^2}{\partial t^2} + F_V \frac{\partial}{\partial t} + k_c & F_\phi \\ G_V \frac{\partial}{\partial t} & \frac{\partial}{\partial t} + G_\phi \end{pmatrix} \begin{pmatrix} X_1 \\ \phi_1 \end{pmatrix} = 0.$$

We denote by $M(\partial/\partial t)$ the matrix operator on the left-hand side of the above equation. The solution is

$$(X_1, \phi_1)^T = A(T) e^{i\omega_c t} u_0 + \text{c.c.}, \quad (11)$$

where $u_0 = (1, z)^T$, with $z = (-i\omega_c G_V)/(G_\phi + i\omega_c)$, is the null right eigenvector of $M(i\omega_c)$, c.c. denoting the complex conjugate. Note that the null left eigenvector of $M(i\omega_c)$ is $u_0^* = (1, -F_\phi/(G_\phi + i\omega_c))$.

At $\mathcal{O}(\varepsilon^2)$, we obtain

$$\begin{pmatrix} M \frac{\partial^2}{\partial t^2} + F_V \frac{\partial}{\partial t} + k_c & F_\phi \\ G_V \frac{\partial}{\partial t} & \frac{\partial}{\partial t} + G_\phi \end{pmatrix} \begin{pmatrix} X_2 \\ \phi_2 \end{pmatrix} = \frac{1}{2} \begin{pmatrix} -F_{VV} \dot{X}_1^2 - 2F_{V\phi} \dot{X}_1 \phi_1 - F_{\phi\phi} \phi_1^2 \\ -G_{VV} \dot{X}_1^2 - 2G_{V\phi} \dot{X}_1 \phi_1 - G_{\phi\phi} \phi_1^2 \end{pmatrix},$$

whose right hand side is rewritten with the help of the first order solution (11) in the form

$$A^2 e^{2i\omega_c t} \underbrace{\begin{pmatrix} \omega_c^2 F_{VV}/2 - i\omega_c z F_{V\phi} - z^2 F_{\phi\phi}/2 \\ \omega_c^2 G_{VV}/2 - i\omega_c z G_{V\phi} - z^2 G_{\phi\phi}/2 \end{pmatrix}}_{\text{denoted } Y_2} + \text{c.c.} + |A|^2 \underbrace{\begin{pmatrix} -\omega_c^2 F_{VV} - i\omega_c(\bar{z} - z)F_{V\phi} - z\bar{z}F_{\phi\phi} \\ -\omega_c^2 G_{VV} - i\omega_c(\bar{z} - z)G_{V\phi} - z\bar{z}G_{\phi\phi} \end{pmatrix}}_{\text{denoted } Y_0}.$$

A particular solution of the second order problem is thus

$$(X_2, \phi_2)^T = A^2 e^{2i\omega_c t} [M(2i\omega_c)]^{-1} \mathbf{Y}_2 + \text{c.c.} + |A|^2 [M(0)]^{-1} \mathbf{Y}_0. \quad (12)$$

In the following, we use the notation $\mathbf{W}_l = [M(il\omega_c)]^{-1} \mathbf{Y}_l$ for $l = 0$ or 2 ; the j th component of \mathbf{W}_l is denoted W_{lj} . Consequently, at $\mathcal{O}(\varepsilon^3)$, there is a resonant term. It is found that

$$\begin{pmatrix} M \frac{\partial^2}{\partial t^2} + F_V \frac{\partial}{\partial t} + k_c & F_\phi \\ G_V \frac{\partial}{\partial t} & \frac{\partial}{\partial t} + G_\phi \end{pmatrix} \begin{pmatrix} X_3 \\ \phi_3 \end{pmatrix} = e^{i\omega_c t} \begin{pmatrix} \lambda \\ v \end{pmatrix} + \text{non-resonant terms},$$

where we have

$$\lambda = -(F_V + 2i\omega_c M)A_T - k_2 A - \gamma_F A |A|^2, \quad (13)$$

$$v = -(z + G_V)A_T - \gamma_G A |A|^2, \quad (14)$$

with $A_T \equiv dA/dT$ and

$$\begin{aligned} \gamma_F &= 2\omega_c^2 W_{21} F_{VV} + i\omega_c (W_{02} - W_{22} + 2\bar{z}W_{21}) F_{V\phi} + (zW_{02} + \bar{z}W_{22}) F_{\phi\phi} \\ &+ 1/2 [i\omega_c^3 F_{VVV} + \omega_c^2 (2z - \bar{z}) F_{VV\phi} + i\omega_c z (2\bar{z} - z) F_{V\phi\phi} + \bar{z}z^2 F_{\phi\phi\phi}], \end{aligned} \quad (15)$$

$$\begin{aligned} \gamma_G &= 2\omega_c^2 W_{21} G_{VV} + i\omega_c (W_{02} - W_{22} + 2\bar{z}W_{21}) G_{V\phi} + (zW_{02} + \bar{z}W_{22}) G_{\phi\phi} \\ &+ 1/2 [i\omega_c^3 G_{VVV} + \omega_c^2 (2z - \bar{z}) G_{VV\phi} + i\omega_c z (2\bar{z} - z) G_{V\phi\phi} + \bar{z}z^2 G_{\phi\phi\phi}]. \end{aligned} \quad (16)$$

A solution at $\mathcal{O}(\varepsilon^3)$ exists if the Fredholm condition is satisfied:

$$u_0^* \begin{pmatrix} \lambda \\ v \end{pmatrix} = 0.$$

Hence this condition, corresponding to the elimination of resonant terms, finally gives the amplitude equation

$$\delta dA/dT = \alpha A + \beta A |A|^2,$$

with coefficients

$$\delta = F_\phi (z + G_V) - (G_\phi + i\omega_c)(F_V + 2i\omega_c M) = 2\omega_c [M\omega_c - i(F_V + MG_\phi)], \quad (17)$$

$$\alpha = k_2 (G_\phi + i\omega_c), \quad (18)$$

$$\beta = (G_\phi + i\omega_c)\gamma_F - F_\phi \gamma_G. \quad (19)$$

Now, using the usual decomposition of the complex amplitude $A(T) = |A| \exp(i\theta)$, we may rewrite the amplitude equation as

$$\begin{cases} d|A|/dT = (\Gamma|A| + \Lambda|A|^3)/2, \\ d\theta/dT = (\Omega + \chi|A|^2)/2, \end{cases} \quad (20)$$

in which the coefficients are defined by

$$\Gamma = 2 \operatorname{Re}(\alpha/\delta), \quad \Lambda = 2 \operatorname{Re}(\beta/\delta), \quad \Omega = 2 \operatorname{Im}(\alpha/\delta) \quad \text{and} \quad \chi = 2 \operatorname{Im}(\beta/\delta). \quad (21)$$

Substituting (17) and (18), we obtain the following relatively simple formulae:

$$\Gamma = -\frac{4\omega_c^2 F_V}{|\delta|^2} \left(\frac{k - k_c}{\varepsilon^2} \right) \equiv -2\bar{\Gamma} (k - k_c) / \varepsilon^2$$

and

$$\Omega = \frac{4\omega_c [F_V G_\phi + M(G_\phi^2 + \omega_c^2)]}{|\delta|^2} \left(\frac{k - k_c}{\varepsilon^2} \right) \equiv 2\bar{\Omega} (k - k_c) / \varepsilon^2.$$

The coefficients Λ and χ cannot in general be expressed in such a simple way, except when Dieterich–Ruina friction laws are considered. Having obtained these analytic expressions in terms of derivatives of F and G , it is straightforward to evaluate the coefficients in the amplitude equation for any given friction law. Direct comparison with the experimental results of Heslot et al. is possible since (20) indicates the typical amplitude of oscillations expected, and the dependence of oscillation amplitude with physical parameters. A stable limit cycle exists if $\Gamma > 0$ and $\Lambda < 0$ and has a constant amplitude given by

$$|A_c|^2 = -\Gamma/\Lambda. \quad (22)$$

Then the phase θ evolves linearly in time according to $d\theta/dT = (\Omega - \Gamma\chi/A)/2$ which implies a frequency shift of $\varepsilon^2(\Omega + \chi|A_c|^2)/2$ from ω_c . The constant amplitude solution of (20) leads to

$$X_1(t) = 2|A_c|\cos[(\omega_c - (\bar{\Omega} + \chi\bar{\Gamma}/A)(k_c - k))t].$$

As a consequence, the maximum perturbation of slip is

$$\max|x - x_0| \approx 2\varepsilon|A_c| = (4\omega_c/|\delta|)(-F_V/A)^{1/2}(k_c - k)^{1/2} \quad (23)$$

and, differentiating, we find that

$$\max|\dot{x} - V| \approx 2\varepsilon|A_c|[\omega_c - (\bar{\Omega} + \chi\bar{\Gamma}/A)(k_c - k)] \quad (24)$$

for the maximum perturbation of slip rate. As we will discuss later on, these two equations are very useful to estimate the effect of inertia on the amplitude, once a particular friction law is considered. In particular, we shall see that the expression (23) is of great interest in estimating the apparent critical stiffness \hat{k} that would be estimated from a certain experimental precision or noise level of order Δx . Supposing that the experimental measurement error is $\Delta x \approx \max|x - x_0|$, we would find that

$$\hat{k} = k_c + \frac{|\delta|^2 A}{16\omega_c^2 F_V} (\Delta x)^2. \quad (25)$$

This expression shows that the critical stiffness \hat{k} for the onset of stick-slip oscillations arising from a supercritical Hopf bifurcation would be underestimated with an error of order $|\delta|^2 A \Delta x^2 / (16\omega_c^2 F_V)$ in the presence of measurement error or noise level Δx . Informally, the error or noise means that the oscillation is not detected until its amplitude reaches Δx , resulting in a downwards shift of the estimated location of the bifurcation point. With careful measurement, extrapolation of data using (23) enables this influence to be corrected, but we stress here that this problem is particularly sensitive to such errors (see Fig. 4(b)). Note that Eq. (25) can also be seen as the iso-level curves of stick-slip amplitude Δx in the (V, k) phase diagram. We will show that such effects might explain the discrepancy in Heslot et al.'s experiments between the minimum of the friction coefficient and the observed complex transition at large slip rates.

3. Application to the Dieterich–Ruina friction laws

In this section we review two simple widely used forms of rate-and-state friction law and compute analytically the corresponding coefficients of the weakly nonlinear analysis. Comparisons with the numerical computation of bifurcation diagrams are also provided.

3.1. Definition

The Dieterich–Ruina friction laws are of the Amontons–Coulomb type

$$F(\dot{x}, \phi) = \sigma\mu(\dot{x}, \phi),$$

in which the dynamical friction coefficient is defined by

$$\mu(\dot{x}, \phi) = a_v + a\ln(\dot{x}/V_*) + b\ln(V_*\phi/L). \quad (26)$$

As suggested by experiments (Dieterich, 1978, 1979; Ruina, 1980, 1983), the interfacial state ϕ has to reach a steady state over a characteristic length scale L and must satisfy an evolution law $(1)_2$ such that, when the sliding is stationary, the dynamical friction coefficient (26) varies logarithmically with the slip rate according to

$$\mu_{ss}(V) = a_v - b_v\ln(V/V_*). \quad (27)$$

Experimentally, it is observed that the steady-state friction coefficient has a purely velocity-weakening form over a wide range of slip rate. In the experiments of Heslot et al., it is found that $a_v = 0.369$, $b_v = 0.014$ and $V_* = 0.9 \times 10^{-6} \text{ m s}^{-1}$ (cf. Table 1). Fig. 4(a) shows the corresponding steady-state friction coefficient.

Two main evolution laws for the state variable ϕ have been proposed. They are commonly known as “Dieterich’s slowness law” (ageing law) and “Ruina’s slip law.”¹ In the former law, defined by

$$G(\dot{x}, \phi) = -1 + |\dot{x}|\phi/L, \quad (28)$$

the state variable is interpreted as a characteristic contact lifetime (Dieterich, 1978, 1979; Ruina, 1983; Heslot et al., 1994; Marone, 1998) where L is a constant memory length (of the order of μm for paper). This law has the advantage of reproducing the logarithmic evolution with the time of stick of the static friction coefficient as observed experimentally (Dokos, 1946; Dieterich, 1978). On the contrary, Ruina’s slip law obeying

$$G(\dot{x}, \phi) = (|\dot{x}|\phi/L)\ln(|\dot{x}|\phi/L) \quad (29)$$

¹ The terms “ageing law” and “slip law” are sometimes used, respectively, for (28) and (29) (e.g. Rice, 1983; Rice and Ben-Zion, 1996). In this article, we follow the terminology of the review article of Marone (1998) and refer to them as the Dieterich law and the Ruina law.

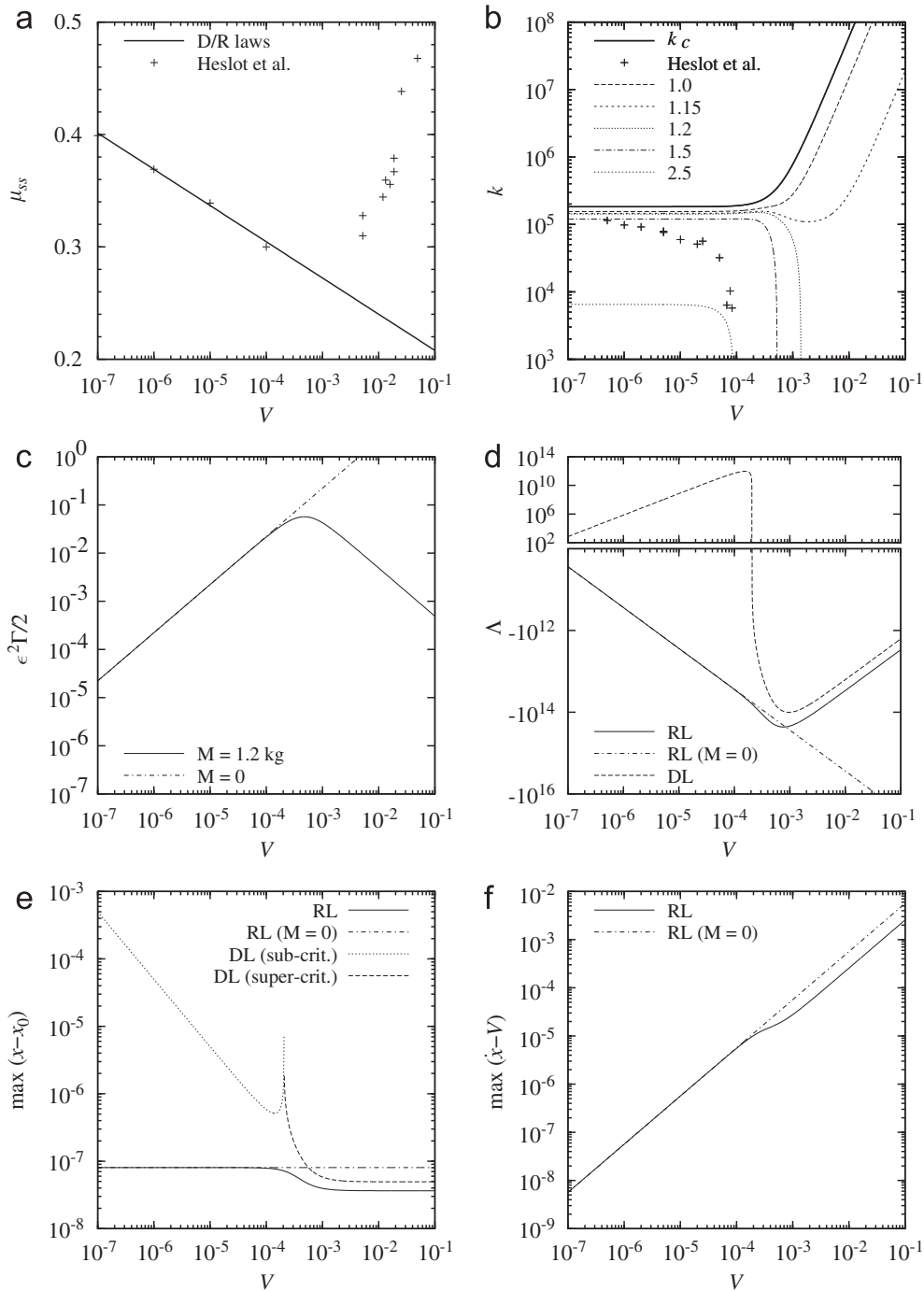


Fig. 4. Results for the Dieterich–Ruina laws—(a) steady-state dynamical friction coefficient vs. Heslot et al.’s experimental data; (b) critical stiffnesses k_c and \hat{k} for different values of Δx (in μm); (c) instability growth rate for $M = 1.2$ kg (—) and $M = 0$ kg (---); (d) Landau coefficient Λ ; (e) slip perturbation amplitude; (f) slip rate perturbation for the Ruina law. The growth rate (c) and amplitudes (e), (f) are estimated at a distance $k_c - k = 0.001k_c$ from criticality. In the legends, RL and DL refer to the Ruina law and Dieterich law, respectively.

Table 1
Parameter values used to fit the experimental data of Heslot et al. (1994).

a_v	a	b	b/a	$b_v = b - a$	L (m)	V_* (ms^{-1})
0.369	0.0349	0.0489	1.4011	0.014	0.9×10^{-6}	10^{-6}

does not strengthen in truly stationary contact but requires slip to evolve. But, in both cases, the response to a jump in slip rate takes a slip of the order of the characteristic length L , that is, a time $\tau_\phi = L/V$, so that the interfacial steady state is $\phi_{ss} = L/V$.

For these laws the critical stiffness (3) of the stick-slip onset takes the form

$$k_c = \frac{\sigma(b-a)}{L} \left(1 + \frac{MV^2}{La\sigma} \right). \quad (30)$$

As a result, the inertia promotes instability by increasing k_c in comparison with its constant value $\sigma(b-a)/L$ in the quasi-static regime, thus widening the stick-slip domain (see Fig. 4(b)). As noted by Roy and Marone (1996) for instance, this departure from the quasi-static value is significant when $MG_\phi/F_V \gg 1$, that is, for slip rates such that

$$V \gg \sqrt{a\sigma L/M} \equiv \hat{V} \approx 5.6 \times 10^{-4} \text{ m s}^{-1}. \quad (31)$$

3.2. Results and discussion

Beginning with the coefficient Γ , we note that it does not depend on whether G is given by (28) or (29) because their first partial derivatives evaluated at a steady state are the same. It is found that

$$\Gamma_{DR} = -k_2 \frac{\sigma a/V}{(\sigma a/V)^2 + M[M(b/a)(V/L)^2 + 2\sigma a/L]}. \quad (32)$$

Without inertia ($M = 0$), the growth rate $\varepsilon^2 \Gamma/2$ of the instability increases linearly with the slip rate: $\Gamma_{DR} = -k_2 V/(\sigma a)$ (recall $k_2 < 0$). However, (32) clearly shows that the presence of inertia decreases the growth rate of the instability which then attains a maximum of

$$\Gamma_{DR}^{\max} = \frac{\frac{3\sqrt{3}}{4} \sqrt{-a + \sqrt{a(a+3b)}}}{3b - a + \sqrt{a(a+3b)}} \sqrt{\frac{bL}{\sigma a M}}$$

at a slip rate $V = \sqrt{(-a + \sqrt{a(a+3b)})/(3b)} \hat{V} \approx 0.552 \hat{V}$, in the conditions of the experiments of Heslot et al. (cf. Table 1). Fig. 4(c) shows this non-monotonic variation of the growth rate of the instability at a distance from onset of $k_c - k = 0.001 k_c$. For both the Dieterich and Ruina laws, the inertia thus has a subtle destabilising effect by opening the domain of instability towards larger spring stiffness (cf. Fig. 4(a)) in combination with a drop in growth rate, slowing down the development of stick-slip. It should be noticed that the maximum of the growth rate arises at slip rates comparable with the ones at which complex dynamics was observed by Heslot et al.

Concerning the Landau coefficient \mathcal{A} , we find that

$$\mathcal{A}_D(V) = \frac{\sigma M(b-a)^2 V^3 [-M^2(4b+3a)V^4 - 6L\sigma a^2 MV^2 + L^2 \sigma^2 a^3]}{L^2(M^2 b V^4 + 2L\sigma a^2 MV^2 + L^2 \sigma^2 a^3)[M^2(4b-3a)V^4 + 2L\sigma a^2 MV^2 + L^2 \sigma^2 a^3]} \quad (33)$$

when we consider the Dieterich law (28). This expression immediately shows that inertia plays an important role. Indeed, as found by Baumberger et al. (1995) and Ranjith and Rice (1999), neglecting inertia implies that $\mathcal{A}_D(V) = 0$, which would, in turn, require consideration of higher orders in the weakly nonlinear analysis to understand the nonlinear dynamics of the Hopf bifurcation. The present analysis shows that the consideration of inertia is crucial here.

In addition, asymptotically, the expression (33) proves that \mathcal{A}_D changes sign as the slip velocity V varies: as $V \rightarrow 0$ we obtain $\mathcal{A}_D(V) \sim [M(b-a)^2 V^3]/(\sigma L^4 a^3) > 0$, whereas $\mathcal{A}_D(V) \sim -[\sigma(b-a)^2(4b+3a)]/[ML^2 b(4b-3a)V] < 0$ as $V \rightarrow \infty$ (recall that $b > a > 0$, see Table 1). The analysis of the polynomial in the numerator of (33) implies that this change of sign arises at a critical slip rate

$$V_D^* = \sqrt{(-3a + 2\sqrt{a(3a+b)})/(3a+4b)} \sqrt{\hat{V}}, \quad (34)$$

where \hat{V} is defined in (31). Below (resp. above) this value, $\mathcal{A}_D > 0$ (resp. < 0) and the Hopf bifurcation is subcritical (resp. supercritical) (see Figs. 4(d) and 5). Thus, the Dieterich law cannot explain why the experiment of Heslot et al. (1994) seems to show a subcritical Hopf bifurcation at large slip velocity. Nevertheless, the Dieterich law illustrates nicely that our hypothesis of a change in nature with the slip rate of the Hopf bifurcation is possible.

From the Ruina law (29), we obtain

$$\mathcal{A}_R(V) = \frac{\sigma(b-a)V(L\sigma a + MV^2)[M^2(14ab + 3a^2 - 18b^2)V^4 - 2MaL\sigma(b^2 - ab + a^2)V^2 - a^4 \sigma^2 L^2]}{2L^2(M^2 b V^4 + 2L\sigma a^2 MV^2 + L^2 \sigma^2 a^3)[M^2(4b-3a)V^4 + 2L\sigma a^2 MV^2 + L^2 \sigma^2 a^3]}. \quad (35)$$

This expression shows that $\mathcal{A}_R(V) < 0$ for all slip velocities; at low velocities we have $\mathcal{A}_R(V) \sim -(b-a)V/(2aL^3) < 0$ as $V \rightarrow 0$, and at high velocities we have $\mathcal{A}_R(V) \sim [\sigma(b-a)(14ab + 3a^2 - 18b^2)]/[2MbL^2(4b-3a)V] < 0$ as $V \rightarrow \infty$, and the discriminant of the quartic expression in V on the numerator of (35) is $\Delta = -4M^2 \sigma^2 L^2 a^2 (b-a)(4a^3 + 16a^2 b + ab^2 - b^3)$, which is negative at least for the values shown in Table 1, cancelling the possibility of having a change of sign of \mathcal{A}_R . Thus, the Ruina

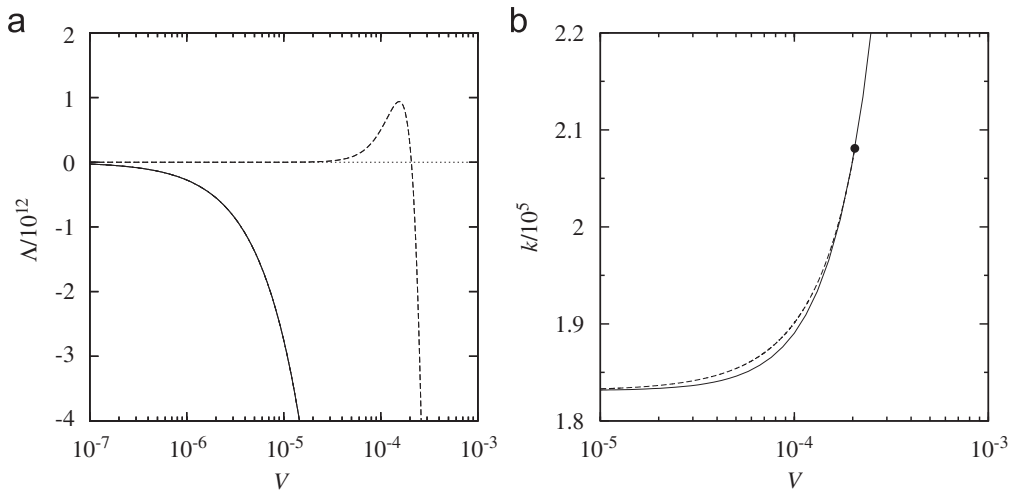


Fig. 5. A detailed look at the Dieterich–Ruina laws—(a) Landau coefficients: Ruina law (—), Dieterich law (- - -); (b) regime diagram for the Dieterich law: Hopf bifurcation locus (—) (critical stiffness curve k_c), saddle-node bifurcation locus (- - -). The Hopf bifurcation is supercritical for large V and subcritical for small V . The location of the saddle-node bifurcation meets the Hopf bifurcation locus line (•) at $k \approx 2.08 \times 10^5$ N and $V \approx 2.31 \times 10^{-5}$ m s $^{-1}$ where A changes sign. The saddle-node bifurcation converges towards k_c as V decreases. Note that Fig. 6 shows the bifurcation diagrams at $V = 10^{-4}$ m s $^{-1}$.

law produces a supercritical Hopf bifurcation and is unable to induce a change of its nature as we would require to explain the observations of Heslot et al. (1994).

Nevertheless, considering the amplitude of the limit cycle, we see that inertia reduces the stick-slip magnitude slightly from its inertialess value (compare the solid and dot-dashed lines in Fig. 4(e)). Noting that $A_R(V) = -(b - a)V/(2aL^3)$ for the inertialess system, the supercritical nature of the Hopf bifurcation is preserved. This confirms the early result of Gu et al. (1984) who showed that a quasi-static spring–block system is unstable (*resp.* stable) for $k < k_c$ (*resp.* $k > k_c$) for small perturbations. Moreover, as $\Gamma_{DR} = -k_2V/(\sigma a)$ for $M = 0$, we have from (23) $\max|x - x_0| \approx 2\sqrt{2/(b - a)}L^{3/2}\sigma^{-1/2}(k_c - k)^{1/2}$, which shows that the slip amplitude scales like the memory length according to

$$\max|x - x_0| \sim \varepsilon L$$

from a distance $k_c - k = \varepsilon^2 k_c$ to criticality. This illustrates the control of stick-slip at onset due to the memory effects and the sensitivity to measurement errors and noise level for the experimental determination of k_c that inertia renders even more challenging to measure.

Our analytical results are confirmed and completed by computing bifurcation diagrams with the continuation software AUTO (Doedel et al., 1991). Fig. 6 illustrates the subcritical nature of the Hopf bifurcation in the case of the Dieterich law in comparison with the supercritical bifurcation implied by the Ruina law for a driving velocity of $V = 10^{-4}$ m s $^{-1}$. On the branch of oscillatory solutions, depicted by the maximum and minimum amplitude of limit cycles at Fig. 6, we see that the slip rate at which the turning point occurs, leading to a stable limit cycle, is close to the value of the slip rate of the Hopf bifurcation. Continuation in the two parameters (V, k) of the location of this limit point shows that it disappears at V_c and tends towards the critical curve $k_c(V)$ (the Hopf bifurcation location) as the driving velocity decreases (as shown in Fig. 5(b)). As V decreases, the amplitude of oscillation at the turning point increases; nevertheless, the difference in amplitude of the stable limit cycles, close to, and far from, the Hopf bifurcation, is not significant. Fig. 7 indeed shows similar trends for the two laws while plotting the relative magnitude (*i.e.* the difference between the maximum and minimum amplitudes of a periodic orbit, relatively to the steady state) of the spring force, slip, slip rate and period. Note that all these quantities decrease as the driving speed V rises at fixed stiffness. We can thus conclude that it might be very difficult to distinguish experimentally the Dieterich law from the Ruina one.

Now, we discuss the effect of inertia in more detail. Again, in both cases, we know that it induces at large V a deviation from the constant value of k_c (Eqs. (3) and (30); Fig. 4(b)). In addition, the numerical continuation of the periodic orbits shows that the amplitude increases very rapidly as $|k - k_c|^{1/2}$ close to the onset of instability as expected, before evolving as a power law in the stiffness while k is reduced. This behaviour has been attributed to a relaxation oscillation regime controlled by inertia by Putelat et al. (2008), where further details can be found. The bifurcation diagrams plotted in Fig. 7 suggest that noise or measurement error in an experiment could lead to an incorrect location of the Hopf bifurcation when inertia is important. For instance, roughly speaking, considering Figs. 7(c) and (d) shows that a noise naturally produced during an experiment driven at 10^{-3} m s $^{-1}$ and larger than μ m in slip amplitude could lead to an error in the measurement of k_c . The noise level would obscure stick-slip oscillations of smaller amplitude. A noise of order 10μ m would mask the inertial effect on k_c . Thus a shift towards smaller stiffnesses should be observed. In fact, the weakly nonlinear analysis,

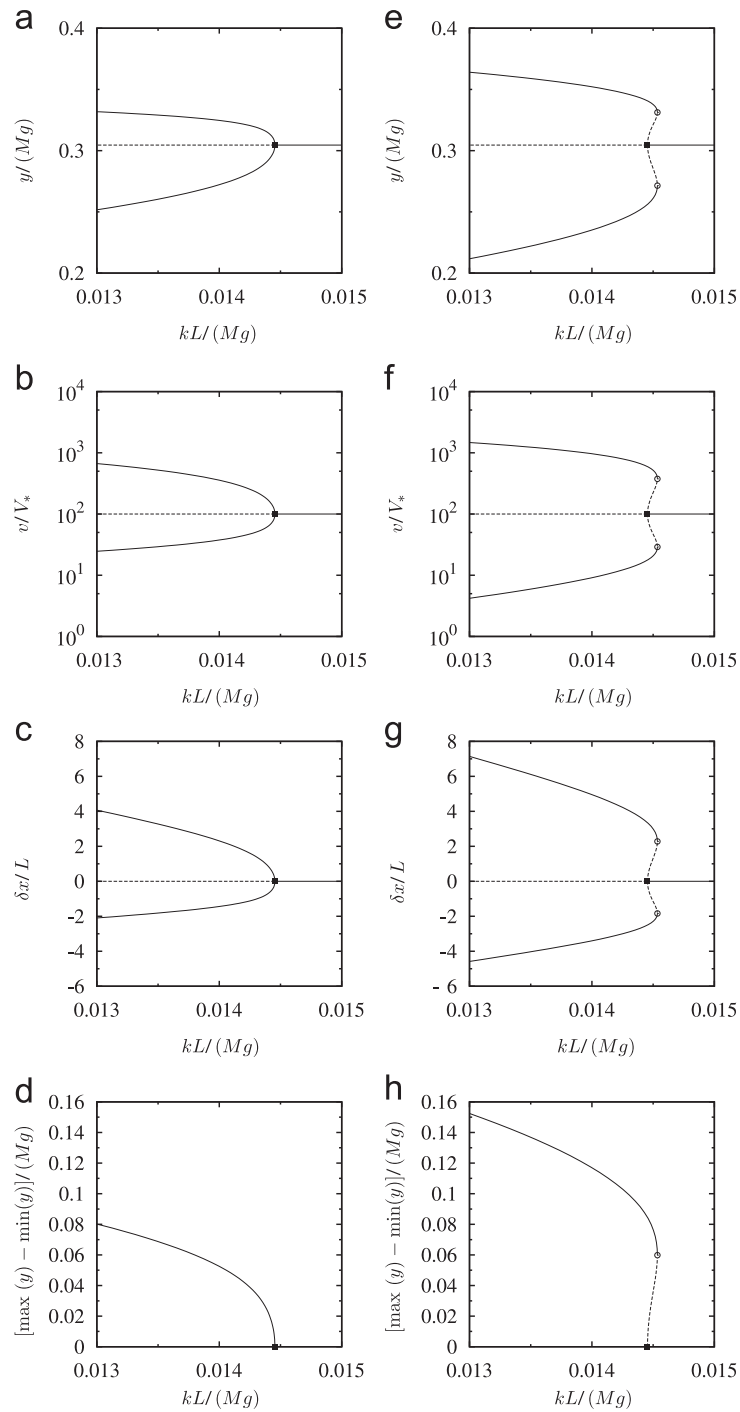


Fig. 6. Bifurcation diagrams for the Ruina law (a–d) and Dieterich law (e–h). The maximum and minimum amplitudes of the limit cycles, born at the Hopf bifurcation point (■), are plotted for: (a, e) the spring force, (b, f) the slip rate, (c, g) the slip distance and (d, h) the stress drop. Solid (dotted) lines read for stable (unstable) solutions. The symbol ◆ denotes the saddle-node bifurcation. The bifurcation diagrams are computed with the continuation software Auro for a driving velocity $V/V_* = 10^2$, considering the stiffness as continuation parameter. Note the change in nature of the Hopf bifurcation in the case of the Dieterich law.

through the formula (25), gives an interesting quantitative estimation of the sensitivity to inertia of the apparent critical stiffness \hat{k} . In addition to the critical curve k_c , Fig. 4(b) shows for the Ruina law how \hat{k} varies quickly with a noise level or measurement error Δx of about $1 \mu\text{m}$. Above this value, \hat{k} becomes concave and restricts the apparent domain of stick-slip to low values of V and k ; an inertialess system leading to

$$\hat{k}|_{M=0} - k_c = -\frac{\sigma(b-a)}{8L^3}(\Delta x)^3.$$

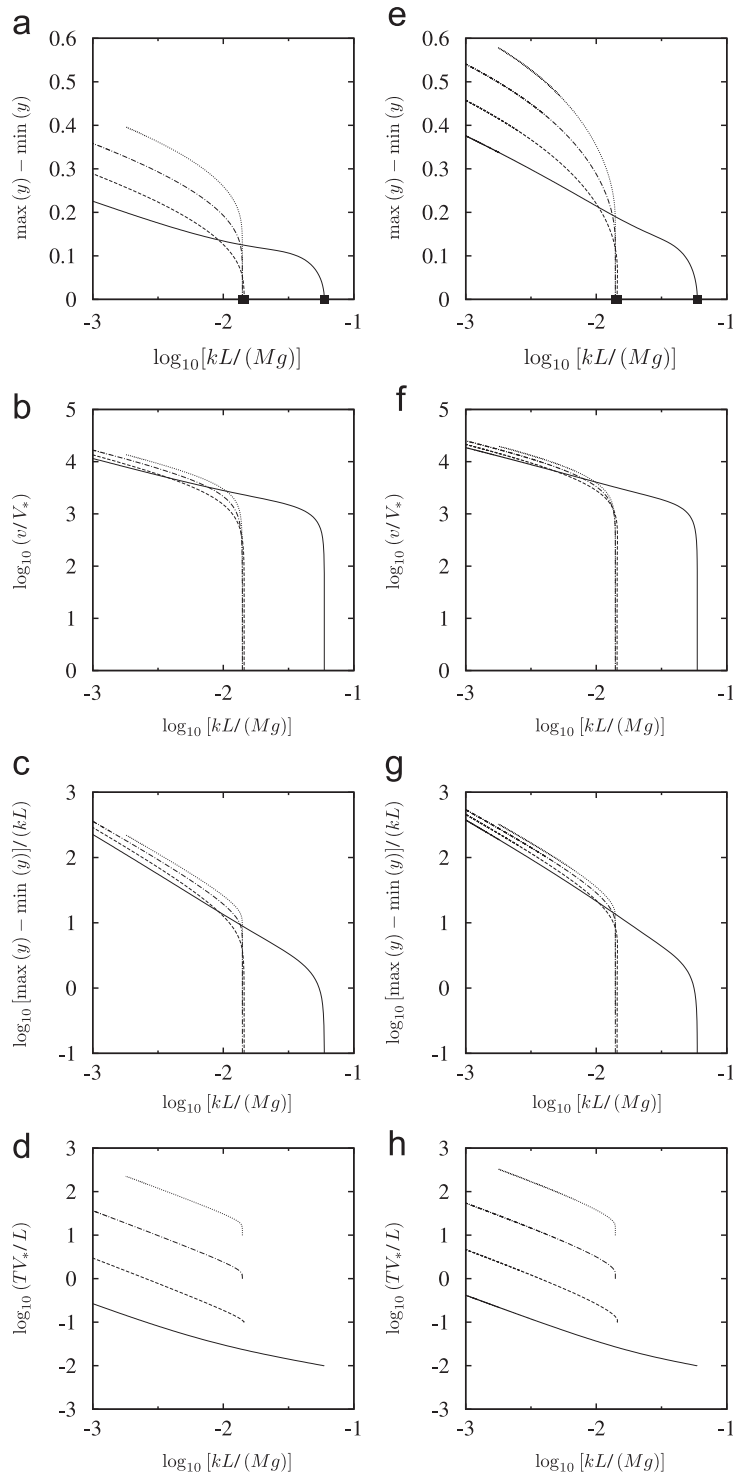


Fig. 7. Comparison of the magnitudes (i.e. the difference between the maximum and minimum amplitudes) of the limit cycles for the Ruina law (a–d) and Dieterich law (e–h). Four driving velocities are displayed: $V/V_* = 1000$ (—); $V/V_* = 100$ (- - -); $V/V_* = 10$ (- · - · -); $V/V_* = 1$ (· · · ·). Recall $V_* = 10^{-6} \text{ m s}^{-1}$.

This is related to the diminution of stick-slip amplitudes due to inertia (cf. Fig. 4(e)). This phenomenon could give an explanation of the discrepancy pointed out in the experiment of Heslot et al. (1994). It should be noted, however, that they reported a noise level for displacement of $10^{-2} \mu\text{m}$.

Finally, we note that the subcritical nature of the Hopf bifurcation at small slip rate induced by the Dieterich law could lead to hysteretic dynamics. This would be a natural explanation for the complexity of slip history observed by Rice (1994) in the elastodynamic modelling of a strike-slip fault when using the Dieterich law; in contrast, the Ruina law would lead to periodic events (see also Rice and Ben-Zion, 1996).

4. Application to a spinodal friction law

In this section we introduce and discuss a modified friction law, first proposed by Putelat et al. (2007), and investigate the results of the weakly nonlinear analysis of Section 2.2 when applied to this modified friction law.

4.1. Definition

In addition to their monotonic nature, the most significant drawbacks of the Dieterich–Ruina laws are the logarithmic singularity of Eq. (26) when $v \rightarrow 0$, an unlimited decrease of the steady-state coefficient with the velocity and the absence of saturation of the state at large time in the particular case of the ageing law (28).

A way to avoid the logarithmic singularity was proposed by Rice and Ben-Zion (1996), Ben-Zion and Rice (1997) and Lapusta et al. (2000) in considering

$$\mu(\dot{\chi}, \phi) = a \sinh^{-1} \left\{ \frac{\dot{\chi}}{2V_*} \exp \left[\frac{a_v + b \ln(V_* \phi / L)}{a} \right] \right\}. \quad (36)$$

Such an expression can be fully derived from assuming a thermally activated rate process which describes the local creep of interfacial asperity contacts (Heslot et al., 1994; Rice et al., 2001). According to this point of view, the rate-and-state dependence of friction supposes that the interfacial slip rate follows from a transition-state Eyring process whose energy barrier $E_*(\phi)$ evolves with the state of the interface and which must overcome, for slip to occur, with the help of applied stress and thermal noise. Combining forward and backward jumps over the effective energy barrier, such a microscopic mechanism leads to the generic frictional slip rate

$$v = 2V_* \exp \left(\frac{-E_*(\phi)}{k_B T} \right) \sinh \left(\frac{\tau}{a\sigma} \right),$$

where k_B is the Boltzmann constant, T the absolute temperature and $a = k_B T / \Omega \sigma_c$. The symbols Ω and σ_c refer to a volume of activation and an average normal stress borne at the asperity contacts. In this framework, the reference slip rate V_* is interpreted as the product of the average slip due to one jump over the energy barrier and the frequency of jump attempts. Expression (36) is formally obtained with $E_*(\phi) = \Omega \sigma_c [a_v + b \ln(V_* \phi / L)]$.

Recently, Putelat et al. (2007) modified expression (36), by taking $E_*(\phi) = \Omega \sigma_c [a_v + b \ln(c + \phi / \phi_*)]$, to give

$$\mu(\dot{\chi}, \phi) = a \sinh^{-1} \left[\frac{\exp(a_v/a)}{2} \frac{\dot{\chi}}{V_*} \left(c + \frac{\phi}{\phi_*} \right)^{b/a} \right]. \quad (37)$$

They also modified the state evolution law (1)₂ to

$$G(\dot{\chi}, \phi) = (\phi - 1) / t_{**} + |\dot{\chi}| \phi / L, \quad (38)$$

so that ϕ varies between 0 and 1.² The relations (37) and (38) combine the two competing processes of static ageing and dynamic weakening proposed by Dieterich (1978, 1979). We assume that the former process takes place on a longer time scale, t_{**} , than the latter one, characterised by the relaxation time L/V . The small constant c is introduced in order to give a residual strength to the interface at very high slip rates, when the interfacial state is supposed to have no influence on the friction force with $\phi \approx 0$. The effect is to produce a logarithmic velocity-strengthening at high velocity which agrees qualitatively with the experimental finding of Bureau et al. (2002). For this law, the reference slip rate V_* is associated to the reference state

$$\phi_* = (1 + t_{**} V_* / L)^{-1}.$$

As discussed by Putelat et al. (2007), for small enough steady sliding velocities such that

$$V \ll L / t_{**},$$

the interface remains rough ($\phi \approx 1$) behaving in a velocity-strengthening manner. Consequently, such a modification of (28) results in a local maximum of the steady-state friction force obtained for a slip rate

$$V_M \approx L / [(b/a - 1)t_{**}].$$

Furthermore, choosing $t_{**} \gg L / V_*$ implies that $V_M \ll V_*$ which localises this velocity strengthening/weakening transition at a very low slip rate. It is moreover found that the steady-state friction law has a local minimum at

$$V_m \approx (1 + 1/R)(b/a - 1)V_* / c,$$

² It is remarked that the law (38) can be expressed in the general form

$$G(\dot{\chi}, \phi) = -\frac{1}{t_{**}} \frac{\phi - \phi_{ss}(\dot{\chi})}{\phi_{ss}(\dot{\chi})}$$

as was noted by Estrin and Bréchet (1996), their Eq. (2), with their ageing time t_a non-dimensionalised so that $\phi = t_a / t_{**}$. Whereas Estrin and Bréchet (1996) assume the Dieterich form $t_a^{ss}(\dot{\chi}) = L / \dot{\chi}$ (Dieterich, 1979) but then introduce a cut-off to avoid small $\dot{\chi}$, we have chosen instead to regularise the Dieterich steady-state formula to $\phi_{ss}(\dot{\chi}) = L / (L + \dot{\chi} t_{**})$ so that $\phi_{ss}(\dot{\chi})$ remains finite as $\dot{\chi} \rightarrow 0$.

as a result of introducing the constant c in (37). We denote $R = t_{**}V_*/L$ the ratio of the characteristic time scale of static ageing t_{**} over the dynamic weakening time scale of reference L/V_* . For $c = 10^{-3}$ and the parameter values of Table 1 we find $V_M = 2.493 \times 10^{-8} \text{ m s}^{-1}$ and $V_m = 4.052 \times 10^{-4} \text{ m s}^{-1}$.

In summary, a non-monotonic steady-state friction coefficient, shown in Fig. 8(a), is obtained. By analogy with the isotherms of the pressure–density relation of the van der Waals gas, or the separation of solidifying binary alloy, we describe such a law as “spinodal”.

An important consequence of the existence of the two extrema of $\mu_{ss}(V)$ is to close off the domain of stick-slip in the (V, k) parameter plane at $V = V_M$ and $V = V_m$ for which $k_c = 0$ (see Fig. 8(b)). As a result, the effect of inertia on the critical stiffness is more subtle than in the previous section and depends on the relative location of V_m compared to the slip rate at

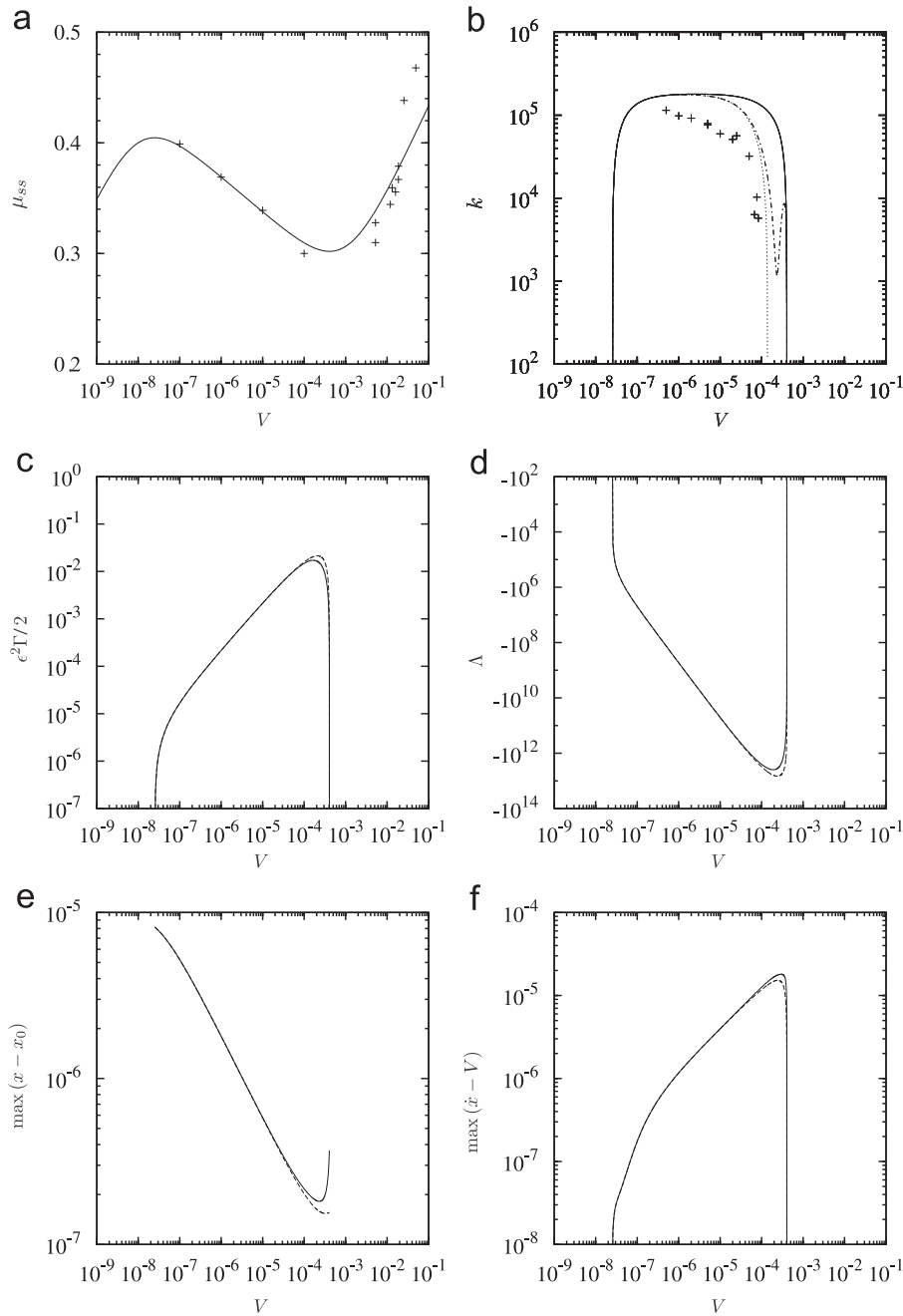


Fig. 8. Results for the spinodal law (37)–(38) with the residual strength parameter $c = 10^{-3}$ —(a) Steady-state friction coefficient; (b) critical stiffness k_c of the stick-slip instability onset (solid line) and apparent critical stiffness \hat{k} for a noise or measure precision of $\Delta x = 5.7 \times 10^{-6} \text{ m}$ (dash-dotted line). The thin dotted line corresponds to \hat{k} for the inertialess system; (c) growth rate of the stick-slip oscillations; (d) Landau coefficient A ; (e) slip perturbation amplitude; (f) slip rate perturbation amplitude. The growth rate (c) and amplitudes (e), (f) are estimated at a distance $k_c - k = 0.001 k_c$ from criticality. Note that the Hopf bifurcation is always supercritical ($A \leq 0$). Symbols: + refers to the experimental results of Heslot et al. in graphics (a) and (b); the lines — and - - - corresponds to $M \neq 0$ and $M = 0$, respectively, in graphics (c)–(f).

which MG_ϕ/F_V becomes order unity, see Eq. (3). For the spinodal law (37), (38), it is straightforward to show that

$$MG_\phi/F_V \approx MV^2/(La\sigma),$$

at large slip rates, as for the Dieterich–Ruina laws. This implies that the condition (31) is still valid. Therefore, the inertia influences k_c only for values of c (which determines V_m) that are smaller than the critical value of c

$$c_{\text{crit}} = \frac{(b/a - 1)V_*}{\sqrt{La\sigma/M}}.$$

For the parameter values used in this study (cf. Table 1), we have $c_{\text{crit}} \approx 7.2 \times 10^{-4}$.

It is important for the sequel to mention that a high-velocity approximation of the spinodal law is

$$\begin{cases} \mu(\dot{x}, \phi) \approx a_* + a \ln(\dot{x}/V_*) + b \ln(c + \phi/\phi_*), \\ \dot{\phi} \approx 1/t_{**} - |\dot{x}|\phi/L, \end{cases}$$

assuming that the interfacial state and slip rate, respectively, remain small and large during stick-slip oscillations; a situation encountered at high-velocity driving. In fact, this approximation is nothing else than the Dieterich law (26), (28) modified by incorporating a high-velocity strengthening behaviour so that

$$\begin{cases} \mu(\dot{x}, \phi) = a_* + a \ln(\dot{x}/V_*) + b \ln(c + \phi V_*/L), \\ \dot{\phi} = 1 - |\dot{x}|\phi/L, \end{cases} \quad (39)$$

once we consider the limit $R \rightarrow +\infty$ and the rescaling of the interfacial state $\phi \rightarrow \phi/t_{**}$. We note that the law (39) was used by Cochard et al. (2003) in the context of the stabilisation of frictional sliding by normal load modulation. A similar law was also proposed earlier by Weeks (1993) but associated with the Ruina slip law (29).

The steady-state form of (39)

$$\mu_{\text{ss}}(V) = a_* + (a - b) \ln(V/V_*) + b \ln(1 + cV/V_*) \quad (40)$$

attains a minimum at

$$V_m(c) = (b/a - 1)V_*/c, \quad (41)$$

and leads to the comprehensive critical stiffness and stick-slip frequency

$$k_c(V, c) = (ac\sigma/L)[V_m(c) - V][1 + MV^2/(a\sigma L)]/(V_* + cV), \quad (42)$$

$$\omega_c(V, c) = (V/L)^2[b/a - 1 - (bc/a)/(V_* + cV)]. \quad (43)$$

We will use the modified Dieterich law (39) to carry out with useful analytical results the interpretation of the results obtained from the spinodal law.

We remark also, before considering the results of the weakly nonlinear analysis, that we should keep in mind the hypothesis that the residual strength parameter c might be a decreasing function of the normal stress (Putelat et al., 2007). It has indeed been observed for rock friction by Kilgore et al. (1993) that the transition at $V = V_m$ from a velocity weakening regime to a velocity strengthening regime is displaced towards higher velocities as the normal stress is increased. This experimental result suggests that a change in the mass of the block used for performing a spring–block experiment will change the location of the local minimum of the friction coefficient.

4.2. Results and discussion

With the material parameters of Table 1 and using the spinodal friction law (37)–(38), we compute numerically the coefficients of the amplitude equation, and other related quantities, as presented in Fig. 8.

We start by analysing the predictions of the weakly nonlinear analysis at constant $c = 0.001$. This value is chosen for a good visual agreement with the measurements of the friction coefficient performed by Heslot et al. (1994) (cf. Fig. 8(a)). It produces a critical stiffness curve $k_c(V)$ with an arch shape as plotted (solid line) in Fig. 8(b). As $c > c_{\text{crit}}$, no deviation due to inertia is noticeable. Note also the discrepancy between the theoretical k_c and the experimental measurements of Heslot et al. (1994). Possible origins of this difference are proposed later in this section.

The existence of the two extrema of $\mu_{\text{ss}}(V)$ means that the coefficients of the amplitude equation are only defined for $V_M \leq V \leq V_m$. In this interval, we find numerically that \mathcal{A} is negative which implies that the Hopf bifurcation is supercritical. We moreover observe that Γ and \mathcal{A} rapidly tend to zero as the slip rate tends to V_M or V_m . Concerning the variations of Γ and \mathcal{A} , Figs. 8(c) and (d) show similar trends as for the Dieterich–Ruina laws (Fig. 4(c) and (d)) in the velocity-weakening regime. Extremal values are also taken close to V_m . But in the case of the spinodal law, these trends interfere with the non-monotonic nature of the steady-state friction law. Note also that inertia has a negative effect in the vicinity of V_m by diminishing the absolute magnitudes of Γ and \mathcal{A} .

However, the behaviour of the slip and velocity amplitudes is different from the Dieterich–Ruina laws in several ways. As the velocity increases, the faster decrease of the Landau coefficient relatively to Γ drives a fast drop of the slip amplitude of the periodic orbit conversely to the Ruina law constant behaviour (Fig. 8(e)). In fact this behaviour recalls that obtained

from the Dieterich law (see Fig. 4(e)) which suggests that it results from the similarity between the evolution laws (28) and (38). Roughly speaking, the higher the driving, the smaller the slip amplitude. Nevertheless we also observe an effect of inertia which slightly increases the slip amplitude in the neighbourhood of V_m . This effect is opposite to the one found for the Ruina law. It is moreover noticeable that the high-velocity slip amplitudes are less than the memory length which suggests a possible sensitivity to noise level or measurement error as discussed for the Dieterich–Ruina laws. About the slip rate fluctuations $\max|\dot{x} - V|$, an equivalent trend exists and consists in an increase of the amplitude with V . Here again inertia enhances the oscillations amplitude, conversely to the Ruina law.

Although it might be difficult to precisely identify experimentally the onset of stick-slip when the amplitude is of same order of magnitude as the noise level, inertia might in fact help the determination of stick-slip onset due to its positive effect on the amplitude. Fig. 8(b) emphasises this conclusion by plotting the apparent critical stiffness \hat{k} (Eq. (25)) for $\Delta x = 5.7 \mu\text{m}$. In the presence of inertia, the apparent stiffness is not displaced towards smaller slip rates as much as without. Actually it is predicted that inertia helps in locating precisely the transition to stick-slip at V_m when using small stiffnesses. Possible mislocation of stick-slip onset is localised around the right-hand shoulder of $k_c(V)$. We also find that the apparent stiffness is rapidly shifted into the domain of stick-slip as soon as $\Delta x > 1 \mu\text{m}$. Thus, we estimate that $1 \mu\text{m}$ is the typical maximum level of noise or experimental error allowed in order to locate accurately the instability threshold in the phase plane. However, Heslot et al. (1994) estimate the measurement error Δx in their experiment to be of order $10^{-2} \mu\text{m}$. So, this explanation is not conclusive, and other reasons for the discrepancy between the present theory and the experiment may be needed. A change in the parameters in the friction law associated with the change in the mass is one possibility. We note meanwhile that the discrepancy between the measurements of k_c and its theoretical location with the spinodal law does not bias our study due to the lack of information available, which prevents us from performing better fits with Heslot et al.'s results.

Figs. 9 and 10 depict the effect of varying the constant c . As c decreases from 10^{-3} to 3×10^{-4} , the local minimum of the friction coefficient moves towards larger slip rates V_m . Consequently, the inertia has an effect on k_c although this does not change the overall trends described above. Fig. 9(a) illustrates how the combined effects of the displacement of V_m and inertia widens the stick-slip domain in the (V, k) - plane. Nevertheless, a significant change is that the Landau coefficient Λ becomes positive in a narrow neighbourhood of V_m (see Fig. 9(b)). The behaviour change that we propose from a supercritical to a subcritical Hopf bifurcation as the driving velocity rises is thus predicted by our spinodal law. Fig. 10(d) shows that inertia is responsible for this change of sign, $\Lambda \leq 0$ for all V when $M = 0$.

The picture given by the weakly nonlinear analysis is completed by numerical investigations using the continuation package AUTO. Figs. 11(a–d) and (e–h), respectively, depict bifurcation diagrams for two different values of c , 10^{-3} and 3×10^{-4} , and the same dimensionless stiffness $\kappa = kL/(Mg) = 10^{-3}$, that is for a stiffness $k = 1.31 \times 10^4 \text{ N m}^{-1}$; $\log_{10}(V/V_*)$ being the continuation parameter. In both cases, the nature of the Hopf bifurcations is confirmed. Near $V = V_m$, a stable limit cycle is born from a supercritical Hopf bifurcation and grows first abruptly and then smoothly as the driving velocity rises. Roughly, the maximum amplitudes are reached in the middle of the velocity-weakening domain. The amplitude decreases next in a monotonic manner for $c = 10^{-3}$ until the supercritical Hopf bifurcation near $V = V_m$ is attained, while the stick-slip orbits become unstable at a saddle-node bifurcation for $c = 3 \times 10^{-4}$. In this case, the limit cycle dies at a subcritical Hopf bifurcation in agreement with the prediction of the weakly nonlinear analysis. It is moreover confirmed that inertia increases the stick-slip amplitude compared to the one obtained for the quasi-static approximation.

Regime diagrams of the spring–block system in spinodal friction are computed by continuation of the loci of the Hopf and saddle-node bifurcations in the two parameters $\log_{10}(\kappa)$ and $\log_{10}(V/V_*)$ using AUTO. Fig. 12 compares the diagrams obtained for four values of the residual strength parameter c . Generically we find a region of bistability, lying between the loci of the Hopf and saddle-node bifurcations, that grows as c decreases. The saddle-node line meets the Hopf bifurcation curve at the codimension-two point $(V^*, k_c(V^*))$. The saddle-node must indeed disappear for $V < V^*$ where $\Lambda < 0$ and the Hopf bifurcation is supercritical. Besides, it is worth noticing that the saddle-node bifurcation does not diverge away from

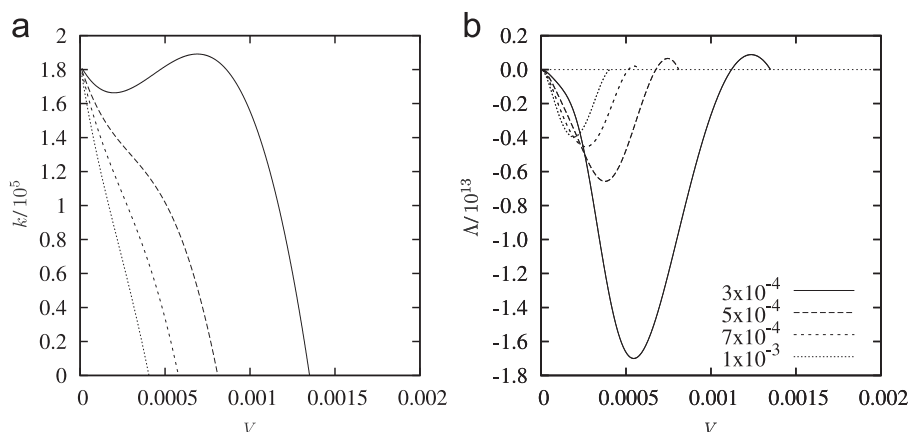


Fig. 9. Effect of the residual strength parameter c on the critical stiffness k_c and the Landau coefficient Λ for the spinodal law (37)–(38).

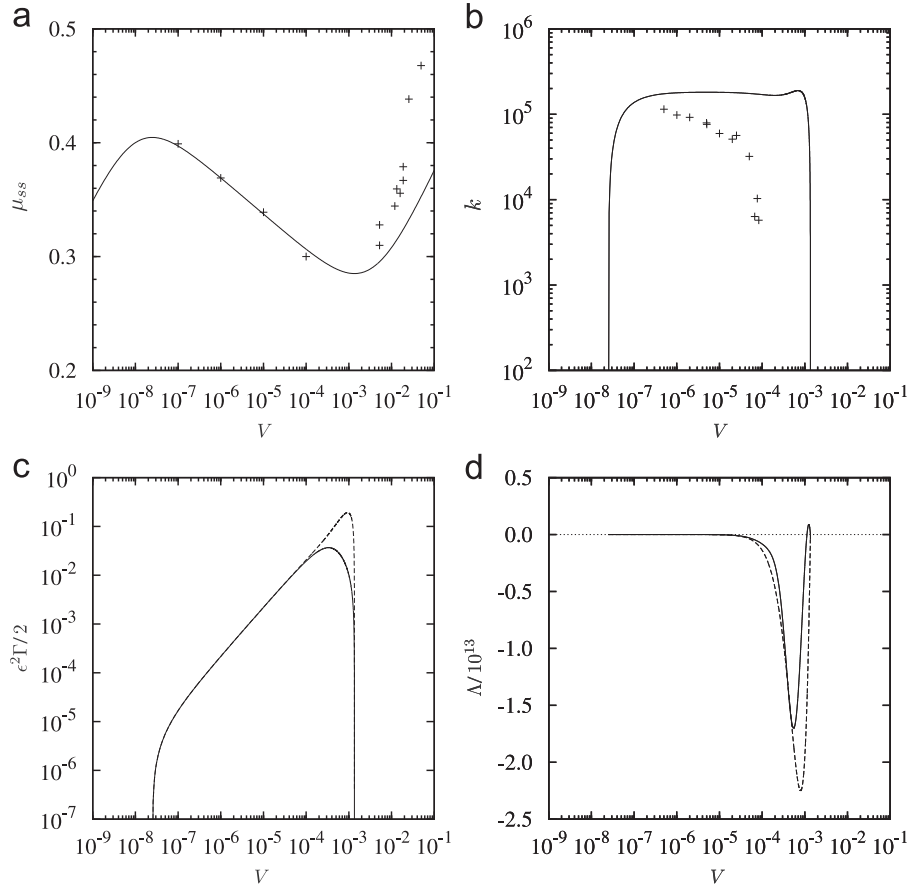


Fig. 10. Results for the spinodal law (37)–(38) with the residual strength parameter $c = 3 \times 10^{-4}$ —(a) Steady-state friction coefficient; (b) critical stiffness k_c of the stick-slip instability onset (solid line); (c) growth rate of the stick-slip oscillations at $k_c - k = 0.001k_c$ from criticality; (d) Landau coefficient A . Note the strong effect of inertia on the sign of A which becomes positive in the vicinity of the local minimum of friction at V_m . Symbols: + refers to the experimental results of Heslot et al. in graphics (a) and (b); the lines — and - - - corresponds to $M \neq 0$ and $M = 0$, respectively, in graphics (c) and (d).

the Hopf bifurcation curve as the stiffness decreases. We observe instead that the bistability domain closes up, the saddle-node line converging tangentially towards the Hopf bifurcation locus at low $\kappa = kL/(Mg)$.³

Analytically, the modified Dieterich law (39) allows a complete understanding of the behaviour change of the Hopf bifurcation and the conditions of existence of the transition velocity V^* . As for the Dieterich law, it is possible to express the amplitude equation's coefficients in a reasonably compact analytical form. We find

$$\Gamma(V) = -k_2 \sigma a^2 L^2 V (cV + V_*) / P_4(V) \quad (44)$$

and

$$A(V) = \frac{ac\sigma V_* V^2 (V - V_m) P_7(V)}{L(cV + V_*)^2 P_4(V) P_5(V)}, \quad (45)$$

where V_m is given by (41) and

$$P_4(V) = bV_* M^2 V^4 + 2a^2 c \sigma L M V^3 + 2a^2 \sigma V_* L M V^2 + a^3 c \sigma^2 L^2 V + a^3 \sigma^2 V_* L^2,$$

$$P_5(V) = 3acLM^2 V^5 + (3a - 4b)V_* LM^2 V^4 - 2a^2 c \sigma L^2 M V^3 - 2a^2 \sigma V_* L^2 M V^2 - a^3 c \sigma^2 L^3 V - a^3 \sigma^2 V_* L^3,$$

$$\begin{aligned} P_7(V) = & (6ab + 6a^2)c^2 L^2 M^3 V^7 + (-4b^2 + 3ab + 9a^2)cV_* L^2 M^3 V^6 \\ & + ((-4b^2 + ab + 3a^2)V_*^2 L^2 M^3 + (3a^2b + 7a^3)c^2 \sigma L^3 M^2)V^5 + (13a^3 - 6a^2b)c\sigma V_* L^3 M^2 V^4 \\ & + ((6a^3 - 6a^2b)\sigma V_*^2 L^3 M^2 + (a^3b - 4a^4)c^2 \sigma^2 L^4 M)V^3 + (3a^3b - 5a^4)c\sigma^2 V_* L^4 M V^2 \\ & + ((a^3b - a^4)\sigma^2 V_*^2 L^4 M - a^5 c^2 \sigma^3 L^5)V - a^5 c \sigma^3 V_* L^5. \end{aligned}$$

The transition velocity V^* is defined by $A(V^*) = 0$ and then corresponds to a zero of the polynomial P_7 . Starting from $V = V_m \approx 1.337 \times 10^{-3}$, we solve $P_7(V^*) = 0$ numerically by iteration. For $c = 3 \times 10^{-4}$, we find $V^* \approx 1.109 \times 10^{-3} \text{ m s}^{-1}$

³ These special periodic orbits are “canard” solutions (Arnold et al., 1999; Guckenheimer et al., 2000) of system (5), (37) and (38).

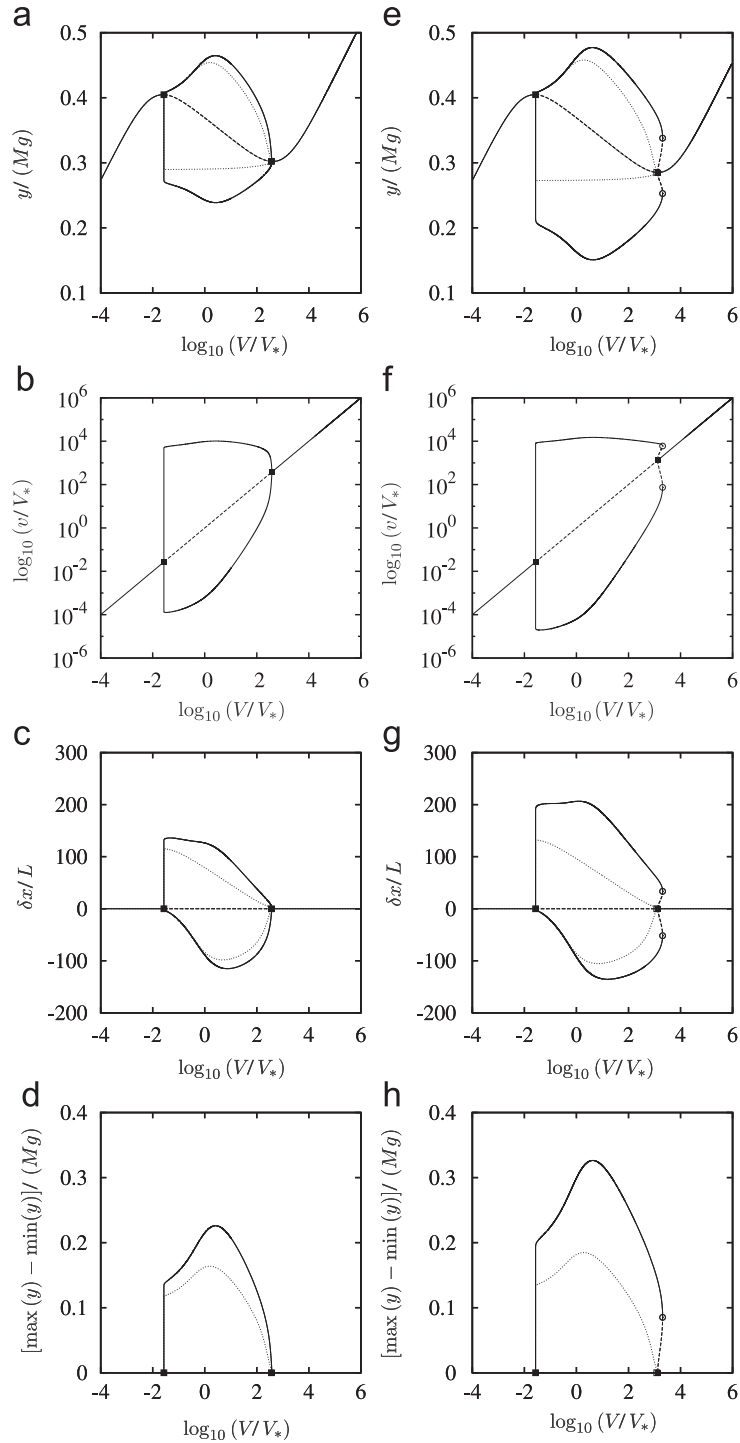


Fig. 11. Bifurcation diagrams of the spring–block system under the spinodal law (37)–(38) for two values of the residual strength parameter $c = 10^{-3}$ (a–d) and $c = 3 \times 10^{-4}$ (e–h)—The maximum and minimum amplitudes of the limit cycles, born at the Hopf bifurcation point (■), are plotted for: (a,e) the spring force, (b,f) the slip rate, (c,g) the slip distance and (d,h) the stress drop. Solid (dotted) lines reads for stable (unstable) solutions. The symbol ▲ denotes the saddle-node bifurcation. The thin dotted line symbolises the amplitudes of the inertialess system. The bifurcation diagrams are computed with the continuation software *AUTO* for a dimensionless stiffness $\kappa = kL/(Mg) = 10^{-3}$, considering the driving velocity as continuation parameter.

(cf. Fig. 13(a)). Repeating this numerical procedure for different values of the residual strength gives the dependence $V^*(c)$ plotted at Fig. 13(b). For small enough values of c , the transition velocity exists, being less than $V_m(c)$, and decreases as c^{-1} , being parallel to $V_m(c)$. Just before $c = 10^{-3}$, V^* curves itself to cross $V_m(c)$ at $c = c^*$. This critical value c^* is the value of the residual strength above which the transition velocity V^* does not exist, the Hopf bifurcation staying supercritical for all velocity between V_M and V_m . As $V_m(c^*) = V^*$ by definition, the critical residual strength must solve $P_7[V_m(c^*)] = 0$, which corresponds to a cubic equation for c^{*2}

$$a_6 c^{*6} + a_4 c^{*4} + a_2 c^{*2} + a_0 = 0,$$

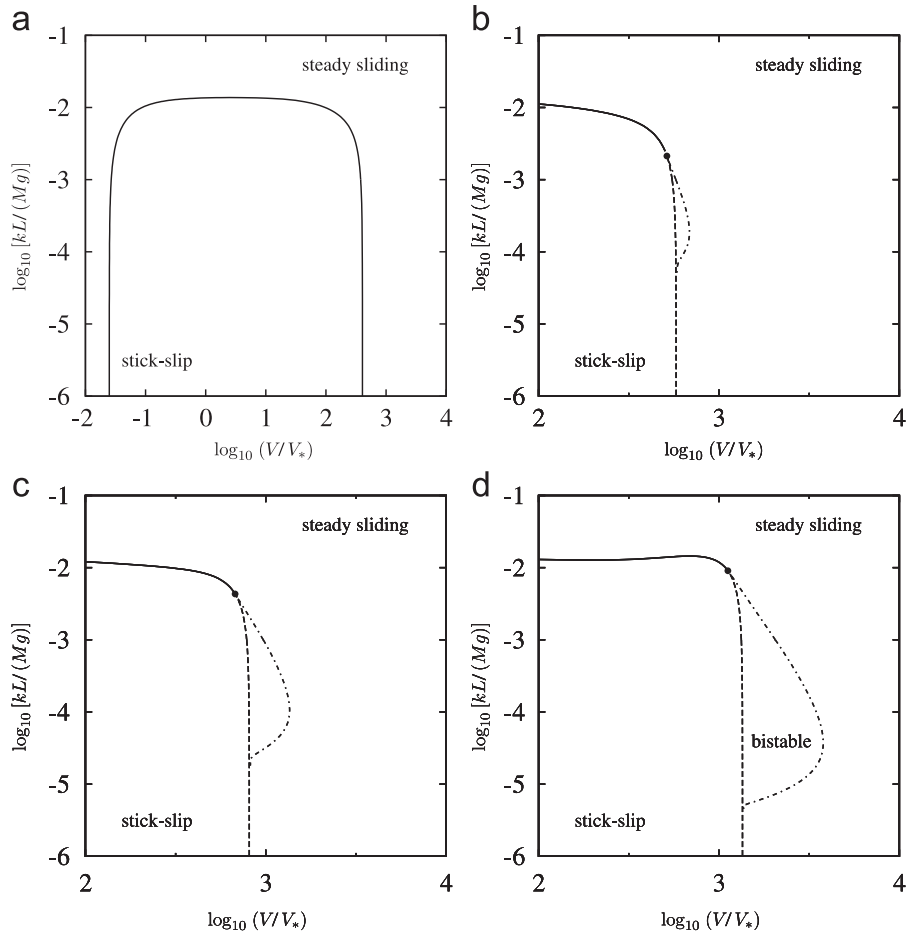


Fig. 12. Regime diagrams of the spring-block system under the spinodal law (37)–(38) for different values of the residual strength parameter: (a) $c = 10^{-3}$; (b) $c = 7 \times 10^{-4}$; (c) $c = 5 \times 10^{-4}$; (d) $c = 3 \times 10^{-4}$. Symbols: the solid and dashed lines, respectively, denotes the supercritical and subcritical Hopf bifurcations, the dash-dotted line is the locus of the saddle-node bifurcation, their intersection symbolised by \bullet . Between the bifurcations is defined a domain of bistability where steady-state and oscillatory slidings co-exist.

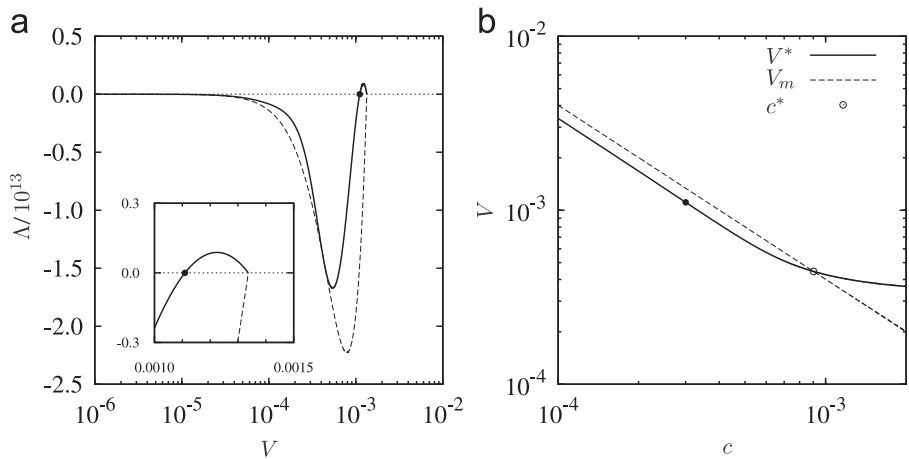


Fig. 13. (a) Landau coefficient (45) of the modified Dieterich law (39) with $c = 3 \times 10^{-4}$. The dashed line refers to the inertialess coefficient, the symbol \bullet locates the transition velocity V^* at which Δ changes sign. (b) Residual strength dependence on the transition velocity V^* (solid line). The dashed line corresponds to $V_m(c)$ given by (41). The bullet symbol \bullet indicates the location of V^* for $c = 3 \times 10^{-4}$, the open circle defines the critical residual strength c^* above which V^* is undefined preventing the behaviour change of the Hopf bifurcation.

whose coefficients are defined by

$$a_0 = b(b-a)^6(2b-a)V_*^7L^2M^3, \quad a_2 = a^3b(b-a)^4(3b-2a)\sigma V_*^5L^3M^2, \quad a_4 = a^6b(b-2a)(b-a)^2\sigma^2V_*^3L^4M,$$

$$a_6 = -a^{10}b\sigma^3V_*L^5.$$

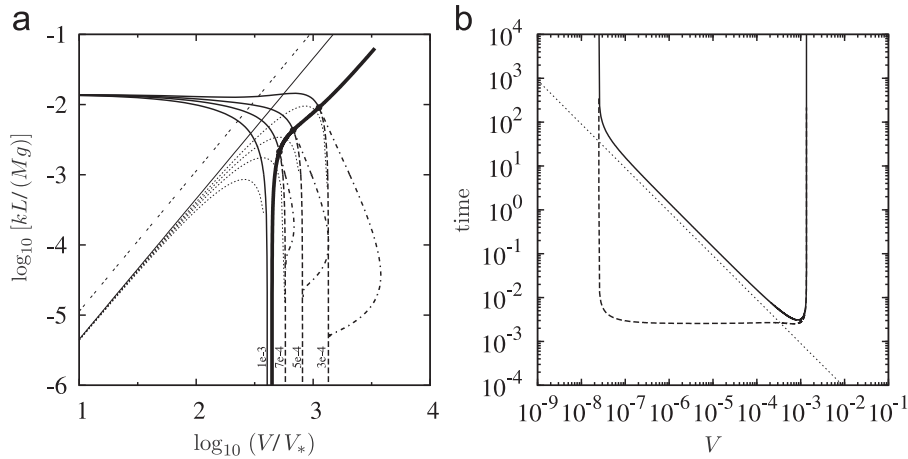


Fig. 14. (a) The transition line $k^*(V^*)$ (thick solid line) divides the parameter space (V, k) between a region on the left where the Hopf bifurcation is supercritical from a region on the right where the bifurcation is subcritical and gives birth to a bistability domain which grows as the residual strength c decreases. The double-dash line corresponds to the quasi-static/inertial regime crossover based on the balance $M/k = (L/V)^2$, whereas the correct inertial domain is located under the border $k = M\omega_c^2$ symbolised by the thin dotted line (the thin solid line corresponds to this latter balance computed for the Dieterich–Ruina laws). The frequency corresponds to the modified Dieterich law (39) and is given by (43). (b) Characteristic time scales for the spinodal law: $1/\omega_c$ (solid line), $(M/k_c)^{1/2}$ (dashed line), L/V (dotted line).

Solving numerically the cubic gives $c^* \approx 9.02 \times 10^{-4}$. Although the analytical expression of c^* can be written in principle, it is easier to find bounds. Balancing a_4c^4 and a_0 gives an upper bound, whereas the balance of a_6c^6 and a_2c^2 leads to a lower bound. We find

$$\frac{(b-a)^4(3b-2a)M^2V_*^4}{a^7\sigma^2L^2} \leq c^{*4} \leq \frac{(b-a)^4(2b-a)M^2V_*^4}{a^6(2a-b)\sigma^2L^2},$$

that is $8.80 \times 10^{-4} \leq c^* \leq 9.52 \times 10^{-4}$.

Combining now the transition velocity $V^*(c)$ obtained numerically with the critical stiffness formula (42) allows the computation of the transition border $k_c^* = k_c(V^*)$ which delimits the region where the Hopf bifurcation is supercritical from the region where it is subcritical. In Fig. 14 we superpose in the (V, k) -plane such a transition border (thick solid line) to the four previous regime diagrams computed with AUTO corresponding to $c = \{3 \times 10^{-4}, 5 \times 10^{-4}, 7 \times 10^{-4}, 10^{-3}\}$. We obtain a very good agreement between the present approximate analysis and the AUTO computations of the transition points (bullet points) for the spinodal law. Note also that k_c^* is undefined for $c > c^*$ and tends to 0 as $c \rightarrow c^*$, that is at $V_m^* = (b/a - 1)V_*/c^* \approx 4.447 \times 10^{-4}$. We finally stress that considering the Ruina slip law (29) with (39) does not provide such a behaviour change for the Hopf bifurcation which remains always supercritical, despite the residual strength. Once again, the analytical details of the state evolution law are crucial and can be discriminated with the weakly nonlinear analysis.

The change of nature of the stick-slip onset is therefore the consequence of the complex interplay between the block inertia, the high-velocity residual strength of the interface and the dynamic interfacial smoothing which are involved in the mathematical structure of the coefficient A through the high order details of the friction law carried by its partial derivatives with respect to its arguments. We thus conclude that it is incorrect to attribute the behaviour change of the Hopf bifurcation to the crossover between a so-called creep regime to an inertial one based on the comparison of the state relaxation time scale L/V and the inertial scale $(M/k)^{1/2}$. As precisely illustrated in Fig. 14, the transition line $k_c^*(V^*)$ does not correspond to the relation $k = M(V/L)^2$. Even a refinement of such an analysis of order of magnitude does not provide a precise insight for the stick-slip bifurcation behaviour. Indeed one could argue that the creep and inertial regimes should be defined from comparing the inertial time scale $(M/k)^{1/2}$ with the stick-slip time scale at onset ω_c^{-1} . We could then define the creep regime when $(M/k)^{1/2} \ll \omega_c^{-1}$ and the inertial regime conversely, the regime boundary being determined by $k = M\omega_c^2$. This boundary is plotted in Fig. 14(a), considering the expression (43). This shows that the transition point (V^*, k_c^*) belongs to the creep domain and cannot be estimated from this kind of analysis of order of magnitude. From it, in the neighbourhood of V_m , we can only conclude that the inertial, stick-slip and state relaxation time scales are of same order, or at least not well separated at stick-slip onset (cf. Fig. 14(b)). To conclude, the only pertinent analysis of this type would need the development of matched asymptotic approximations of the stick-slip cycle like the one tackled by us (Putelat et al., 2008).

5. Other spinodal friction laws

In this section we briefly discuss two alternative candidates for a spinodal law. Both candidates satisfy the multiplicative decomposition of the friction force according to the ‘‘adhesion model’’ of Bowden and Tabor (1954)

$$F = A_r(\phi)S(\dot{x}), \quad (46)$$

where $A_r(\phi)$ denotes the true area of asperity contact and $S(\dot{\chi})$ a creep shear strength of asperities (see Baumberger and Caroli, 2006 for a recent review). In both cases we consider the Dieterich state evolution law (28).⁴ To simplify our discussion, we give these laws the names “nanoscale contact law” and the “micron-scale contact law” due to the scales to which various authors appeal in their construction. We compute the Landau coefficient for these alternative laws and conclude that neither of these laws yields behaviour which corresponds as closely to the experimental results as that derived using the law (37)–(38).

5.1. A nanoscale contact law

The first alternative spinodal law we consider comes from the critical discussion of physical models and phenomenological arguments proposed by Heslot et al. (1994), Baumberger et al. (1995, 1999), and Berthoud et al. (1999) which were comprehensively summarised and completed by Persson (2000).

We start with a phenomenological approach. In the velocity-weakening regime of friction, Heslot et al. (1994) observed that the stick-slip onset boundary slightly decreases with the driving velocity and consequently they proposed modifying the Dieterich–Ruina law (26) by considering

$$\mu_{ss}(V) = a_v - b_v \ln(V/V_*) + c_v \ln^2(V/V_*).$$

Note, however, that the velocity-strengthening that the additional term $c_v \ln^2(V/V_*)$ induces is not sufficient to reproduce the high speed linear strengthening regime reported by Baumberger et al. (1994) and Heslot et al. (1994). Concerned only with the creep regime, Baumberger et al. (1995) then considered an expression for the instantaneous friction coefficient that can be written in the form

$$\mu(\dot{\chi}, \phi) = a_v + a \ln(\dot{\chi}/V_*) + b \ln(\phi/\phi_*) + c_v \ln^2(\phi/\phi_*), \quad (47)$$

with $b = b_v + a$. Following Persson (2000), a term $\ln^2(\phi/\phi_*)$ could physically be understood as a second order memory effect resulting from the time dependence of real contact area due to the asperity creep activated by the normal pressure in quasi-stationary contact.

On the other hand, a physical description of rate-and-state friction has been proposed by Berthoud et al. (1999) and Baumberger et al. (1999) based on Bowden and Tabor’s decomposition (46). In this formulation, the memory effects determine the real contact area through an evolving state variable representing the average contact time of the interface rejuvenation inferred from the logarithmic time evolution of the static friction force consequence of the surface asperity creep given by $A_r(\phi) = A_0[1 + \alpha \ln(\phi V_*/L)]$ (Berthoud et al., 1999; Persson, 2000). In addition, the friction force directly reacts to variations of the slip velocity upon which the interfacial shear strength depends according to $S(\dot{\chi}) = S_0[1 + \beta \ln(\dot{\chi}/V_*)]$, considering a thermally activated shear-induced creep process localised at the nanometric asperity junctions (Baumberger et al., 1999; Persson, 2000). In fact, such a law introduces a term $-\ln^2(V/V_*)$ which leads to a steady-state friction coefficient $\mu_{ss}(V) = A_0 S_0 [1 + (\beta - \alpha) \ln(V/V_*) - \alpha \beta \ln^2(V/V_*)]$, with the wrong curvature and an increasing function of V for the critical stiffness $k_c(V)$ once $V/V_* > \exp[(\beta - \alpha)/(\alpha\beta)]$.

However, we found that this drawback can be resolved by including in the physical model of Baumberger et al. (1999) the second order term $\ln^2(\phi/\phi_*)$ proposed by Persson (2000) for the state evolution of the true contact area $A_r(\phi)$. Indeed, considering the following friction coefficient:

$$\mu(\dot{\chi}, \phi) = [1 + (b/a_v) \ln(\phi/\phi_*) + a_2 \ln^2(\phi/\phi_*)][a_v + a \ln(\dot{\chi}/V_*)] \quad (48)$$

produces another spinodal law with good phenomenological steady-state features. Note that the additional coefficient a_2 can be expressed in terms of those of expression (47) as $a_2 = c_v/a_v + ab/a_v^2$ and that a regularised version of (48) is

$$\mu(\dot{\chi}, \phi) = a[1 + (b/a_v) \ln(\phi/\phi_*) + a_2 \ln^2(\phi/\phi_*)] \sinh^{-1}(\dot{\chi}/\gamma_0)$$

with $\gamma_0 = 2 \exp(-a_v/a) V_* \ll 1$. The velocity-strengthening regimes at very low $\dot{\chi}$ and very high $\dot{\chi}$ of the corresponding steady-state friction coefficient are caused by a third order term $aa_2 \ln^3(V/V_*)$. The choice of $a_2 = 0.0085$ (equivalently $c_v = -1.4885 \times 10^{-3}$) gives a good fit with the experimental data of Heslot et al. (cf. Fig. 15(a)).

Figs. 15 and 16 summarise results for this spinodal law. It is found that the Landau coefficient changes sign twice over the range of velocity for which friction is velocity-weakening. As shown in Fig. 15(c), this produces two bubbles of bistability associated with subcritical Hopf bifurcations at low and high velocity (see Fig. 15(b)). We observe that the domain of subcriticality extends noticeably inside the velocity-weakening region from the local maximum of the friction coefficient. Besides, the numerical continuation of the periodic orbits at fixed velocity $V/V_* = 1$ reveals moreover that a subcritical Hopf bifurcation would have been detected experimentally due to the high amplitude of the oscillations created in this case (see Fig. 15(a)). Hence, this spinodal law does not fully agree with the behaviour observed by Heslot et al. as the law (37)–(38) does.

⁴ Considering Ruina’s slip law (29) does not change the qualitative features described in this section.

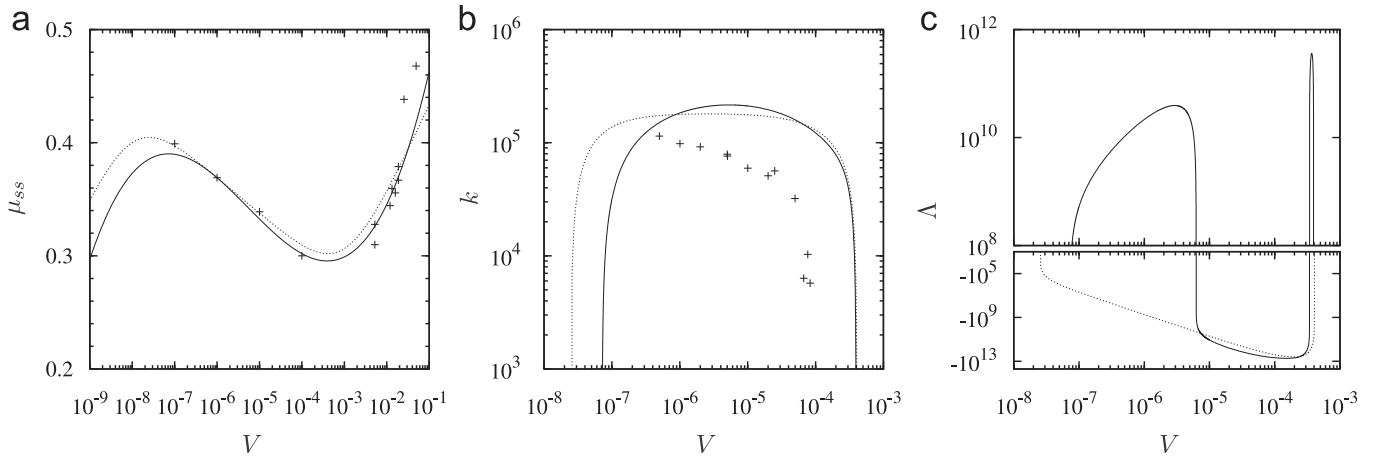


Fig. 15. (a) Steady-state friction coefficient of the nanoscale contact law (48); (b) corresponding critical stiffness k_c (solid line); (c) Landau coefficient Λ . Parameters: $a_1 = 0.369$, $a = 0.0349$, $b = 0.0489$, $a_2 = 0.0085$, $L = 10^{-6}$ m, $V_* = 10^{-6}$ m s $^{-1}$. Note that the Landau coefficient Λ changes sign twice over the whole range of velocity in the velocity-weakening regime of friction. Although $\Lambda \geq 0$ around the local minimum of μ_{ss} , Λ is also positive in $V_M \leq V \leq 6.24 \times 10^{-6}$ implying a subcritical Hopf bifurcation at low velocity in contradiction with the observations of Heslot et al. The behaviour of Λ is thus very sensitive to the analytical details of the friction law: it is possible to discriminate between different candidates of phenomenological friction laws. Symbols: + refers to the experimental results of Heslot et al. in graphics (a) and (b). The thin dotted line corresponds to the law (37)–(38).

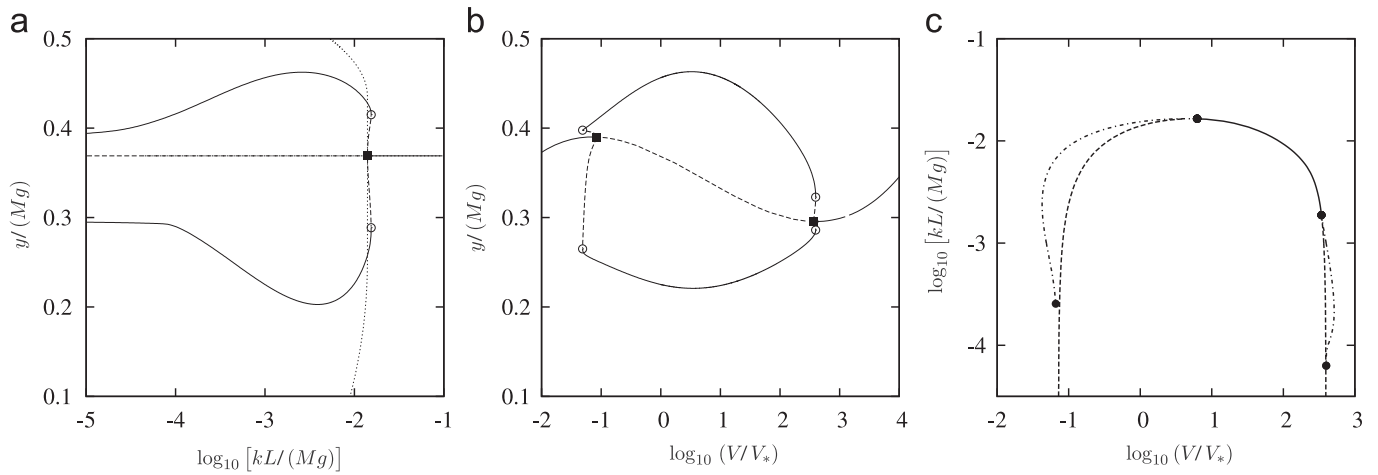


Fig. 16. Numerical continuation results for the nanoscale law (48), $a_2 = 0.0085$ —(a) Bifurcation diagram along the stiffness axis at the driving velocity $V/V_* = 1$; (b) bifurcation diagram along the velocity axis at the stiffness $kL/(Mg) = 10^{-3}$, note the subcritical nature of the Hopf bifurcation, the spinodal shape of (48) prevents the stick-slip amplitude to diverge as the monotonic Dieterich law would do (compare to the thin dotted line in (a)) (see Fig. 11 for symbols definition). (c) Regime diagram: two domains of bistability where steady-state slidings coexist with oscillatory motions as predicted by the weakly nonlinear analysis. Both the numerics and the analysis give a transition velocity at small speed $V_l^* \approx 6.24 \times 10^{-6}$ m 0.16ems $^{-1}$ ($\log_{10}(V_l^*/V_*) \approx 0.7953$) and a transition velocity at high speed $V_h^* \approx 3.41 \times 10^{-4}$ ($\log_{10}(V_h^*/V_*) \approx 2.533$) (see Fig. 12 for symbols definition).

5.2. A micron-scale contact law

Bréchet and Estrin (1994) derived the following expression for the friction coefficient:

$$\mu(t, \dot{x}) = \mu_0 [1 + \mu_1 \ln(1 + t/t_*)] \ln(\dot{x}/V_*),$$

assuming a Nabarro–Herring creep type flow of the contacting asperities,

$$\dot{\varepsilon} = \dot{\varepsilon}_0 \exp(\sigma/\sigma_0), \quad (49)$$

for both the evolution of the asperity junction area induced by the normal pressure and the shearing of asperities during sliding. The time dependence illustrating the ageing of asperities arises from the increase of the junction area associated with the height variation of asperities and results from assuming conservation of volume and constancy of the number of contacts. In contrast to the nanoscopic process referred to by Baumberger et al. (1999), the velocity dependence results from the estimation of the shear rate of the whole asperity as $\dot{\varepsilon} \sim \dot{x}/h_0$, where h_0 is some asperity height. In Estrin and Bréchet (1996), the ageing time t is associated with an ad hoc evolution law of the Dieterich type and must tend to a steady-state value L/V , where L is the average distance between asperities. Note that one argument in favour of replacing the logarithmic velocity dependence with a \sinh^{-1} dependence is that it should be linear in \dot{x} at low shear rates. This corresponds to assuming the Nabarro–Herring creep flow law $\dot{\varepsilon} = \dot{\varepsilon}_0 \sinh(\sigma/\sigma_0)$ (Poirier, 1985) directly in place of (49).

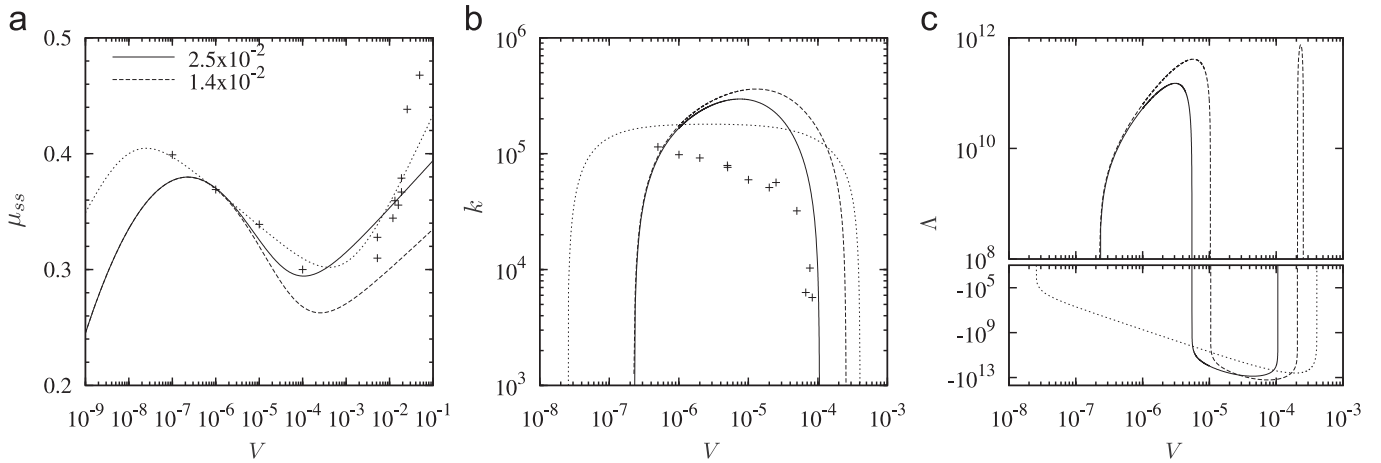


Fig. 17. (a) Steady-state friction coefficient (51) of the micron-scale law (50); (b) corresponding critical stiffness k_c (solid line); (c) Landau coefficient Δ for $c = 2.5 \times 10^{-2}$ and 1.4×10^{-2} . Parameters: $a_v = 0.369$, $a = 0.0349$, $b = 0.0489$, $L = 10^{-6}$ m, $V_* = 10^{-6}$ m s $^{-1}$. Note that the $\Delta \geq 0$ at low velocity in the velocity-weakening regime of friction which implies a subcritical Hopf bifurcation, which conflicts with Heslot et al.'s experiment. The law (51) is, however, able to produce the behaviour change of the Hopf bifurcation at high velocity if the residual strength is small enough. Symbols: + refers to the experimental results of Heslot et al.'s in graphics (a) and (b). The thin dotted line corresponds to the law (37)–(38).

As a result, Bréchet and Estrin (1994) first obtained a dynamic friction coefficient with a spinodal steady-state shape whose both low and high velocity strengthening branch arise from the bulk shearing of asperities, while the velocity-weakening behaviour results from the combination the quasi-stationary ageing and shearing of bulk asperities.

To relate such a law with the classical logarithmic Dieterich–Ruina law (26), we define

$$\begin{cases} \mu(\dot{\chi}, \phi) = a[1 + (b/a_v)\ln(c + V_*\phi/L)] \sinh^{-1}(\dot{\chi}/\gamma_0) \\ \dot{\phi} = 1 - \dot{\chi}\phi/L. \end{cases} \quad (50)$$

where the constant $\gamma_0 = 2\exp(-a_v/a)V_*^5$. The corresponding steady-state law is obviously

$$\mu_{ss}(V) = a[1 + (b/a_v)\ln(c + V_*/V)] \sinh^{-1}(V/\gamma_0). \quad (51)$$

As $\gamma_0 \ll 1$ the instantaneous friction coefficient and its steady-state form can be approximately written as

$$\mu(\dot{\chi}, \phi) \approx a_v + a\ln(\dot{\chi}/V_*) + b\ln(c + V_*\phi/L) + (ab/a_v)\ln(c + V_*\phi/L)\ln(\dot{\chi}/V_*), \quad (52)$$

$$\mu_{ss}(V) \approx a_v + a\ln(V/V_*) + b\ln(c + V_*/V) + (ab/a_v)\ln(c + V_*/V)\ln(V/V_*). \quad (53)$$

Compared to the approximate expressions (39) and (40) of the spinodal law (37)–(38), it is noticeable that the Bréchet–Estrin formulation (50) introduces an additional higher order term whose coefficient ab/a_v is about 10% of the logarithmic terms for the parameter values considered at Table 1. As shown at Fig. 17(a), this is responsible for an additional curvature of the steady-state friction coefficient that renders the fit of Heslot et al.'s experimental data, by tuning the residual strength parameter c , more difficult than for the law (37)–(38). We note in particular that (51) is unable to reproduce correctly the logarithmic velocity-weakening regime for the parameter values considered in the whole paper. Another set of parameter values could, however, be chosen for a better fit of the logarithmic weakening region, but at the expense of the strengthening parts. In any case, the expression (53) will always cause lower values than (40) for the high-velocity strengthening part as $\ln(c + V_*/V)\ln(V/V_*) \approx \ln(c)\ln(V/V_*)$ is negative. This makes the fit of high velocity data more difficult too.

A drawback of the law (50) is the prediction (see Fig. 17) of a subcritical Hopf bifurcation at low velocity which is not consistent with the observations and conclusions of Heslot et al. (1994). Although this behaviour agrees qualitatively with the one produced by the Dieterich law (26)–(28), which is a reasonable approximation of (50) by construction, we find numerically that the curvature of the subcritical Hopf bifurcation is more pronounced leading to relatively large amplitude oscillations (see Figs. 18(a,b)). Such a feature would not have been missed experimentally. Nevertheless (50) predicts the crossover from a supercritical to subcritical Hopf bifurcation at high velocity provided that the residual strength parameter is smaller than a critical value. The phase diagram for the law (50), obtained by numerical continuation, summarises the existence of two bubbles of bistability that these behaviour changes of the Hopf bifurcation produce (Fig. 18(c)).

⁵ Estrin and Bréchet (1996) in fact employed (50)₁ only down to a cut-off velocity v_c below which $\dot{\phi} = 0$. We disregarded this additional feature as it has no effect on the minimum of μ_{ss} .

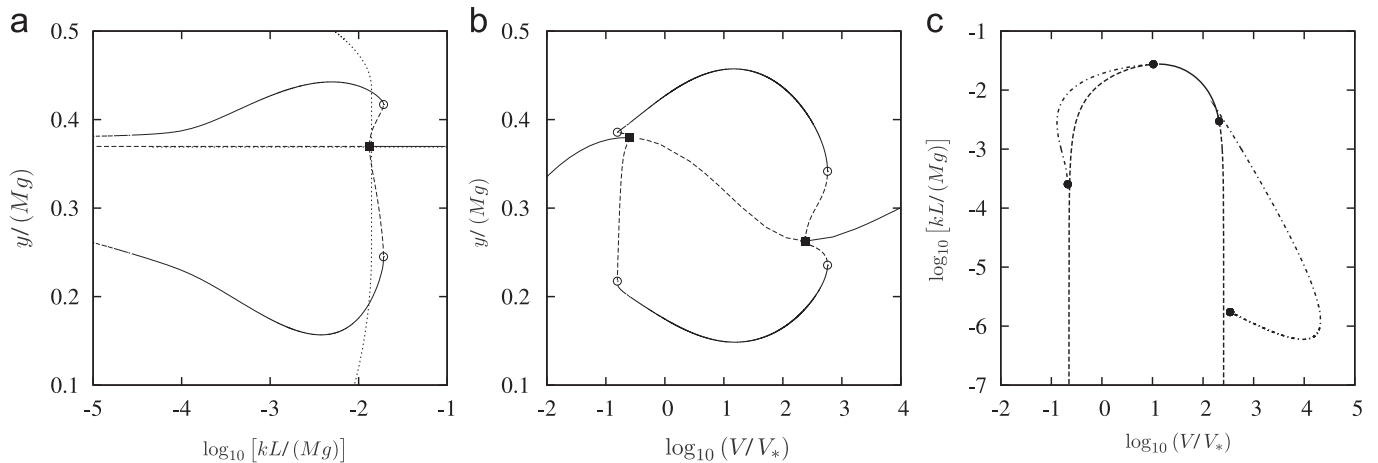


Fig. 18. Numerical continuation results for the micron-scale law (50), $c = 1.4 \times 10^{-2}$ —(a) Bifurcation diagram along the stiffness axis at the driving velocity $V/V_* = 1$, (b) bifurcation diagram along the velocity axis at the stiffness $kL/(Mg) = 10^{-3}$, note the subcritical nature of the Hopf bifurcation, the spinodal shape of (51) prevents the stick-slip amplitude to diverge as the monotonic Dieterich law would do (compare to the thin dotted line in (a)) (see Fig. 11 for symbols definition). (c) Regime diagram: two domains of bistability where steady-state slidings coexist with oscillatory motions as predicted by the weakly nonlinear analysis. Both the numerics and the analysis give a transition velocity at small speed $V_l^* \approx 1.039 \times 10^{-5} \text{ m s}^{-1}$ ($\log_{10}(V_l^*/V_*) \approx 1.01679$) and a transition velocity at high speed $V_h^* \approx 2.07 \times 10^{-4}$ ($\log_{10}(V_h^*/V_*) \approx 2.3179$) (see Fig. 12 for symbols definition).

6. Concluding remarks

The rate-and-state frictional dynamics of a spring–block system has been extensively analysed to identify the effects of inertia on the stick-slip instability onset and further enhance the understanding of the crossover between the creep and inertial regimes of dry friction as described by Heslot et al. In disagreement with these authors, we showed that this transition between the “quasi-static” motion of a spring–block (a designation we prefer as “creep” refers to a deformation mechanism) and its dynamic motion is not directly correlated to the change of monotonicity of the steady-state frictional behaviour from the velocity-weakening regime to the strengthening one. From a weakly nonlinear analysis combined with a fully nonlinear numerical study using the continuation software *AUTO*, we have argued instead that the stick-slip instability, only linearly promoted by the velocity-weakening character of friction, arises from a Hopf bifurcation which may change in nature from supercritical to subcritical as the driving velocity of the spring–block system is increased.

We studied in great detail different friction laws to determine the conditions of such a behaviour change of the stick-slip bifurcation. It turned out that the form of the Landau coefficient in the amplitude equation is very sensitive to the analytical formulation of the friction law and that the weakly nonlinear analysis is thus a powerful and robust possible criterion to discriminate between phenomenological friction laws and suggest which are physically relevant. Indeed, in combination with the numerical computation by continuation methods of spring–block regime diagrams in the parameter plane (V, k) (Figs. 12, 14(a)), it came to light that, amongst the laws studied, only the spinodal law (37)–(38) and its singular high-speed approximation (39) agreed with the observations of Heslot et al. which showed that the Hopf bifurcation changes in nature only once from supercritical to subcritical at a transition velocity V^* slightly smaller than the rheological transition velocity V_m at which friction strengthens again. Precisely, the transition velocity V^* corresponds to a codimension-2 bifurcation point giving birth to a domain of bistability where stable steady-state slidings coexist with large-amplitude oscillatory ones. Bounded by the Hopf and saddle-node bifurcations, this domain overlaps the local minimum of friction $\mu_{ss}(V_m)$ and forms a bubble which starts at the codimension-2 transition point (V^*, k_c^*) where the saddle-node bifurcation disappears to make the Hopf stick-slip bifurcation supercritical for $V < V^*$. Using the law (39) and the weakly nonlinear analysis, we could explain that this domain exists only if the residual strength parameter c , which determines $V^*(c)$ and $V_m(c)$, i.e. the change of monotonicity of the steady-state friction, is less than a critical residual strength parameter c^* defined by the condition $V_m(c^*) = V^*(c^*)$, provided that inertia is also taken into account. For the constitutive parameters of Table 1 we computed $c^* \approx 9.02 \times 10^{-4}$ and $V_m(c^*) \approx 4.447 \times 10^{-4} \text{ m}$. The bubble of bistability closes up at small stiffness tangentially to the Hopf bifurcation line.

In this context, we clearly showed that the Hopf bifurcation changes in nature from supercritical to subcritical in response to the combination of two factors which are (i) the block inertia and (ii) the high-speed residual interfacial strength parameter responsible for the local minimum of steady-state friction. Importantly, we found that an evolution of the interfacial state is also necessary for the behaviour change to happen.⁶ Furthermore, the state evolution law must

⁶ Note that a previous weakly nonlinear study (Elmer, 1997) considered a non-monotonic kinetic friction coefficient only velocity-dependent, disregarding any internal variables. Under this hypothesis, the Hopf bifurcation occurs at the extrema, denoted here V_c , of the friction law and does not depend on the stiffness despite common experimental observations. This situation would correspond in the present work to the artificial constraint that the interfacial state would remain for all time at equilibrium (i.e. on the ϕ -nullcline $\phi = \phi_{ss}(v)$ solution of $G(v, \phi) = 0$) as we could expect in the inertial regime considering a quasi-instantaneous state relaxation due to the separation of time scales $\tau_{cr} \ll \tau_{in}$. With such a constraint, leading to the amplitude at

incorporate a high-velocity dynamic smoothing of Dieterich-type in Eqs. (28) or (38). Instead, considering the spinodal friction coefficient ((37) with a dynamic smoothing of the Ruina-type (Eq. (29)) has been shown to prevent the behaviour change of the Hopf bifurcation.

We emphasise the sensitive role of the interfacial residual strength parameter c in the birth of stick-slip oscillations by determining the local minimum of friction at V_m and the appearance of the bistable domain at V^* associated with small values of $c < c^* \ll 1$. A slight change of c around c^* can have a brutal consequence on the amplitude of stick-slip by switching the Hopf bifurcation from supercritical to subcritical. Recalling that we expect the residual strength to depend on the normal pressure according to the experimental observations of Kilgore et al. (1993), a mass increase should diminish c and then promote subcritical stick-slip transitions. Therefore we point out the necessity of careful experimental studies to clarify the correlation between the location of the local friction minimum and the normal stress imposed to the frictional interface in combination with the nature and position of the stick-slip onset at high velocity. In practice, we expect important consequences of this effect in mechanical engineering and earthquake hazard as it would render the bifurcation dangerous leading to large amplitude instabilities and sensitiveness to finite size perturbation. We warn though that such experimental studies might be challenging as they must be carried out at high velocity where noise might hide the bifurcation location. However, choosing small stiffness and/or large mass should reduce this effect.

Other inertial effects have been observed. Apart from the opening in the stability domain associated with the quadratic divergence in velocity of the critical stiffness, we found that inertia increases the stick-slip amplitude compared to the one that a quasi-static analysis would predict. In relation to Putelat et al. (2008), we stress the importance of the spinodal character of the friction law whose main consequence is to reduce the stick-slip amplitude in comparison with that implied by monotonic laws such as the Dieterich–Ruina laws. As a result, we point out once again the necessity of a careful confrontation of the friction law with experiments in order to obtain a more realistic and physical description of friction. We think indeed that the spinodal law (37)–(38) is a good candidate to achieve this aim.

Acknowledgements

This work has been supported from the Postdoctoral Marie–Curie Individual Fellowship (Contract no. HPMF-CT 2002-01587) and the European Research Network DE.F.I.NO, Deformation and Fracture Instabilities in Novel Materials and Processes (RTN/DEFINO, December 2002–November 2006, HPRN-CT-2002-00198). J.H.P.D. is supported by the Royal Society through a University Research Fellowship. T.P. wishes to thank Philippe Carrière for useful discussions. We are grateful to the two reviewers whose comments stimulated significant improvements of the original draft.

References

- Arnold, V.I., Afrajmovich, V.S., Il'yashenko, Y.S., Shil'nikov, L.P., 1999. *Bifurcation Theory and Catastrophe Theory*. Springer, Berlin.
- Baumberger, T., Heslot, F., Perrin, B., 1994. Crossover from creep to inertial motion in friction dynamics. *Nature* 367, 544–546.
- Baumberger, T., Caroli, C., Perrin, B., Ronsin, O., 1995. Nonlinear analysis of the stick-slip bifurcation in the creep-controlled regime of dry friction. *Phys. Rev. E* 51 (5), 4005–4010.
- Baumberger, T., 1996. Dry friction dynamics at low velocities: experiments on a model system. In: Persson, B.N.J., Tosatti, E. (Eds.), *Physics of Sliding Friction*. Kluwer Academic Publishers, Dordrecht, pp. 1–26.
- Baumberger, T., Berthoud, P., Caroli, C., 1999. Physical analysis of the state- and rate-dependent friction law: dynamic friction. *Phys. Rev. B* 60 (6), 3928–3939.
- Baumberger, T., Caroli, C., 2006. Solid friction from stick-slip down to pinning and aging. *Adv. Phys.* 55, 279–348.
- Ben-Zion, Y., Rice, J.R., 1997. Dynamic simulations of slip on a smooth fault in an elastic solid. *J. Geophys. Res.* 102, 17,771–17,784.
- Berthoud, P., Baumberger, T., G'Sell, C., Hiver, J.-M., 1999. Physical analysis of the state- and rate-dependent friction law: static friction. *Phys. Rev. B* 59 (22), 14313–14327.
- Bowden, F.P., Tabor, D., 1954. *The Friction and Lubrication of Solids*. Clarendon Press, Oxford.
- Bowden, F.P., Freitag, E.H., 1958. The friction of solids at very high speeds: I metal on metal, II metal on diamond. *Proc. R. Soc. A* 248, 350–367.
- Bréchet, Y., Estrin, Y., 1994. The effect of strain rate sensitivity on dynamic friction of metals. *Scr. Met. Mat.* 30, 1449–1454.
- Bureau, L., Baumberger, T., Caroli, C., 2002. Rheological aging and rejuvenation in solid friction. *Eur. Phys. J. E* 8, 331–337.
- Cochard, A., Bureau, L., Baumberger, T., 2003. Stabilization of frictional sliding by normal load modulation. *ASME J. Appl. Mech.* 70, 220–226.
- Dieterich, J.H., 1978. Time-dependent friction and the mechanics of stick-slip. *Pure Appl. Geophys.* 116, 790–806.
- Dieterich, J.H., 1979. Modeling rock friction: 1. Experimental results and constitutive equations. *J. Geophys. Res.* 84, 2161–2168.
- Doedel, E.J., Keller, H.B., Kernevez, J.P., 1991. Numerical analysis and control of bifurcation problems. *Int. J. Bifurcation Chaos* 1 (3), 493–520 AUTO 2000 available via Internet from <http://indy.cs.concordia.ca/auto/>.
- Dokos, S.J., 1946. Sliding friction under extreme pressures. *ASME J. Appl. Mech.* 13A, 148–156.
- Drazin, P.G., 1992. *Nonlinear Systems*. Cambridge University Press, Cambridge.
- Elmer, F.-J., 1997. Nonlinear dynamics of dry friction. *J. Phys. A Math. Gen.* 30, 6057–6063.

(footnote continued)
criticality

$$|A_c|^2 = -\frac{M F''_{ss}(V_c) V - V_c}{k F'''_{ss}(V_c) \varepsilon^2},$$

it does not appear possible for the spinodal laws considered here to produce a change in the bifurcation from supercritical to subcritical as the residual strength is varied; the Hopf bifurcation is always subcritical and no stable oscillation arises. This result strongly suggests that the transient stages of the interfacial state relaxation cannot be neglected to capture the full stick-slip dynamics.

- Estrin, Y., Bréchet, Y., 1996. On a model of frictional sliding. *Pure Appl. Geophys.* 147 (4), 745–762.
- Gu, J.C., Rice, J.R., Ruina, A.L., Tse, S.T., 1984. Slip motion and stability of a single degree of freedom elastic system with rate and state dependent friction. *J. Mech. Phys. Solids* 32, 167–196.
- Guckenheimer, J., Hoffman, K., Weckesser, W., 2000. Numerical computation of canards. *Int. J. Bifurcation Chaos* 10, 2669–2687.
- Heslot, F., Baumberger, T., Perrin, B., Caroli, B., Caroli, C., 1994. Creep, stick-slip, and dry-friction dynamics: experiments and a heuristic model. *Phys. Rev. E* 49, 4973–4988.
- Kilgore, B.D., Blanpied, M.L., Dieterich, J.H., 1993. Velocity dependent friction of granite over a wide range of conditions. *Geophys. Res. Lett.* 20 (10), 903–906.
- Lapusta, N., Rice, J.R., Ben-Zion, Y., Zheng, G., 2000. Elastodynamic analysis for slow tectonic loading with spontaneous rupture episodes on faults with rate-and-state dependent friction. *J. Geophys. Res.* 105 (B10), 23765–23789.
- Lim, Y.F., Chen, K., 1998. Dynamics of dry friction: a numerical investigation. *Phys. Rev. E* 58, 5637–5642.
- Marone, C., 1998. Laboratory-derived friction laws and their application to seismic faulting. *Annu. Rev. Earth Sci.* 26, 643–696.
- Poirier, J.-P., 1985. *Creep of Crystals: High-temperature Deformation Processes in Metals, Ceramics and Minerals*. In: Cambridge Earth Science Series. Cambridge University Press, Cambridge.
- Persson, B.N.J., 2000. *Sliding Friction: Physical Principles and Applications*. NanoScience and Technology, second ed Springer, Berlin.
- Putelat, T., Dawes, J.H.P., Willis, J.R., 2007. Sliding interactions of two frictional interfaces. *J. Mech. Phys. Solids* 55 (10), 2073–2105.
- Putelat, T., Willis, J.R., Dawes, J.H.P., 2008. On the seismic cycle seen as a relaxation oscillation. *Philos. Mag.* 88, 3219–3243 DOI: 10.1080/14786430802216374.
- Rabinowicz, E., 1995. *Friction and Wear of Materials*, second ed Wiley, New York.
- Ranjith, K., Rice, J.R., 1999. Stability of quasi-static slip in a single degree of freedom elastic system with rate and state dependent friction. *J. Mech. Phys. Solids* 47, 1207–1218.
- Rice, J.R., Ruina, A.L., 1983. Stability of steady frictional slipping. *J. Appl. Mech.* 50, 343–349.
- Rice, J.R., 1983. Constitutive relations for fault slip and earthquake instabilities. *Pure Appl. Geophys.* 121, 443–475.
- Rice, J.R., Tse, S.T., 1986. Dynamic motion of a single degree of freedom system following a rate and state dependent friction law. *J. Geophys. Res.* 91 (B1), 521–530.
- Rice, J.R., 1994. Comparison of slip complexity produced by two rate-and-state dependent friction law. *EOS Trans. Am. Geophys. Union* 75 (Suppl. 44), 441.
- Rice, J.R., Ben-Zion, Y., 1996. Slip complexity in earthquake fault models. *Proc. Natl. Acad. Sci. USA* 93, 3811–3818.
- Rice, J.R., Lapusta, N., Ranjith, K., 2001. Rate and state dependent friction and the stability of sliding between elastically deformable solids. *J. Mech. Phys. Solids* 49, 1865–1898.
- Roy, M., Marone, C., 1996. Earthquake nucleation on model faults with rate and state dependent friction: effects of inertia. *J. Geophys. Res.* 101 (B6), 13,919–13,932.
- Ruina, A.L., 1980. *Friction laws and instabilities: a quasistatic analysis of some dry frictional behavior*. Ph.D. Thesis, Brown University.
- Ruina, A.L., 1983. Slip instability and state variable friction laws. *J. Geophys. Res.* 88, 10,359–10,370.
- Scholz, C.H., 2002. *The Mechanics of Earthquakes and Faulting*, second ed Cambridge University Press, Cambridge.
- Shimamoto, T., 1986. Transition between frictional slip and ductile flow for halite shear zones at room temperature. *Science* 231, 711–714.
- Tsutsumi, A., Shimamoto, T., 1997. High-velocity frictional properties of gabbro. *Geophys. Res. Lett.* 24, 699–702.
- Weeks, J.D., 1993. Constitutive laws for high-velocity frictional sliding and their influence on stress drop during unstable slip. *J. Geophys. Res.* 98, 17,637–17,648.